Design and Development of Flexible Sensors Using Non-Conventional Methods

by

Lucas Montgomery Casanova

A Thesis Presented in Partial Fulfillment
of the Requirements for the Degree
Master of Science

Approved April 2018 by the
Graduate Supervisory Committee:

Sangram Redkar, Chair
Thomas Sugar
Bradley Rogers

ARIZONA STATE UNIVERSITY

May 2018

ABSTRACT

In this work, different methods for fabrication of flexible sensors and sensor characterization are studied. Using materials and equipment that is unconventional, it is shown that different processes can be used to create sensors that behave like commercially available sensors. The reason unconventional methods are used is to cut down on cost to produce the sensors as well as enabling the manufacture of custom sensors in different sizes and different configurations. Currently commercially available sensors are expensive and are usually designed for very specific applications. By creating these same types of sensors using new methods and materials, these new sensors will show that flexible sensor creation for many uses at a fraction of the cost is achievable.

ACKNOWLEDGMENTS

I would like to thank my advisor, Dr. Sangram Redkar for giving me the opportunity and helping to guide me through this entire process as well continuing to motivate me and keep me excited and focused. Dr. Redkar would remind me of the importance of never giving up and helping me push through difficult parts of the project, while also providing all the resources I needed to complete work on the project. I am also very thankful to Thomas Sugar, and Bradley Rogers, who were not only instructors of mine but are on my thesis committee and have always made themselves available to help me with anything I needed help with.

My family is a huge part of my success and my main motivation to continue and never give up, without my wife to keep me determined and focused on school while she stayed home raising our son, none of this would have been possible and for that I am greatly thankful to her. Finally, I would like to thank my dad who has always supported every decision I have made and ultimately taught me the importance of getting an education in any field to better my life situation and be able to provide for my family while doing something that I am passionate about. The partial support provided by NextGen Aeronautics is gratefully acknowledged

TABLE OF CONTENTS

Page

Page

LIST OF FIGURES

Figure Page

Page

LIST OF TABLES

Table Page

CHAPTER 1

INTRODUCTION

This thesis presents techniques and characterization of flexible sensors created using non-conventional methods. The motivation for this thesis is discussed in this chapter as well as a history of creating flexible electronics, research on fabrication methods and materials, and the problem statement.

1.1 Motivation

There is a need for flexible and soft electronic devices in applications such as personalized health-monitoring, human motion detection, human-machine interfaces, and soft robotics (Amjadi 1678). Currently there are not standardized methodologies or elements that exist in creating flexible electronics because the emerging technologies are so new (Castano 1). The electronics and sensors that are currently available are rigid, expensive to fabricate, and not customized for specific applications. By creating flexible electronics and sensors using new fabrication processes and materials, the cost for electronics and sensors that can be integrated into wearable technologies for very specific applications will be reduced allowing these devices to be more easily produced and utilized in all emerging fields where conventional electronics are not the best option. Development and characterization of flexible sensors requires research into the history of flexible electronics and methods used to create them.

1.2 History

1.2.1. Early 1900's

In 1902 the first patents on "printed" wiring was filed [Gilleo 2]. This creation of the first circuits were initially originated to solve the needs of

the telephone exchange interconnection system. These first circuits were made by cutting or stamping metal foil into conductive patterns (Gilleo 2). These coper or brass traces would then be bonded to thin, pliable dielectrics using adhesives (Gilleo 2). Albert Hansen, the German scientist and inventor often credited as the “Father of Circuitry”, realized that high density interconnects were greatly important and therefore created his circuits using conductors on both sides. He also realized that the inter-conductor connections were also of great importance and improved upon this idea by adding access holes which allowed the top and bottom conductors to be selectively joined (Gilleo 2). Even more, Hanson came up with and patented multiple layer circuitry, allowing him to achieve even higher conductor density for use in future products (Gilleo 2). Even though more advanced patterning and interconnect processes would take decades to improve upon, the basic flex circuit concepts still in use today came from Hanson’s patents that were filed in Germany and Britain in 1902 and 1903 respectively.

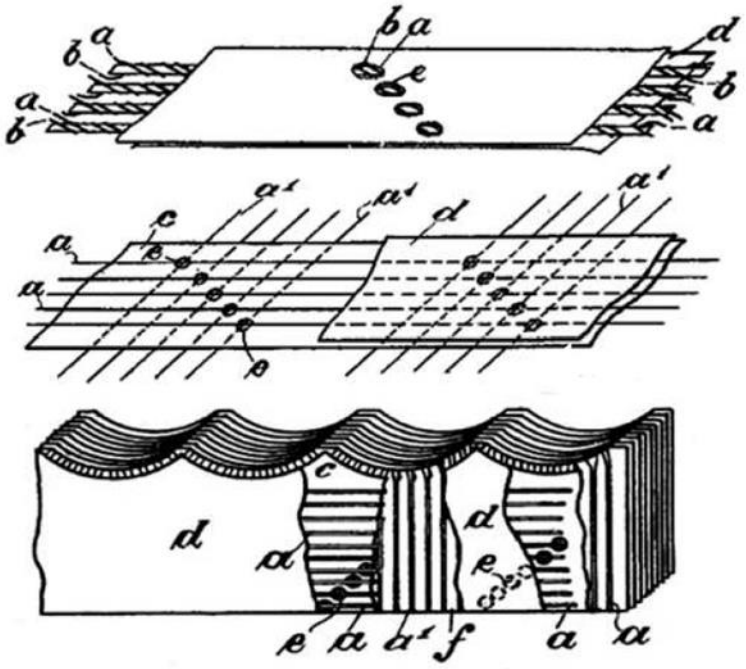

Figure 1: Figures from the first flex circuit patents

The creation of the radio and further improvements in radio technology became an important driver for printed circuitry (Gilleo 2). This need for better printed circuitry in radios saw new processes being developed for circuit creation based on additive and subtractive construction processes (Gilleo 2). By the end of the 1920's most major countries and ships were using wireless Marconi radios (Gilleo 2). Lives were being saved by ships in distress and the Titanic even broadcasted its tragedy using the Marconi wireless (Gilleo 2). The huge success and potential for such technology saw the development of an immense market for mass-producing circuits and inventors and engineers were being highly motivated to respond to the

challenge (Gilleo 2). One of the most important aspects of this growing technology, however, was the fact that essentially all of the circuits and

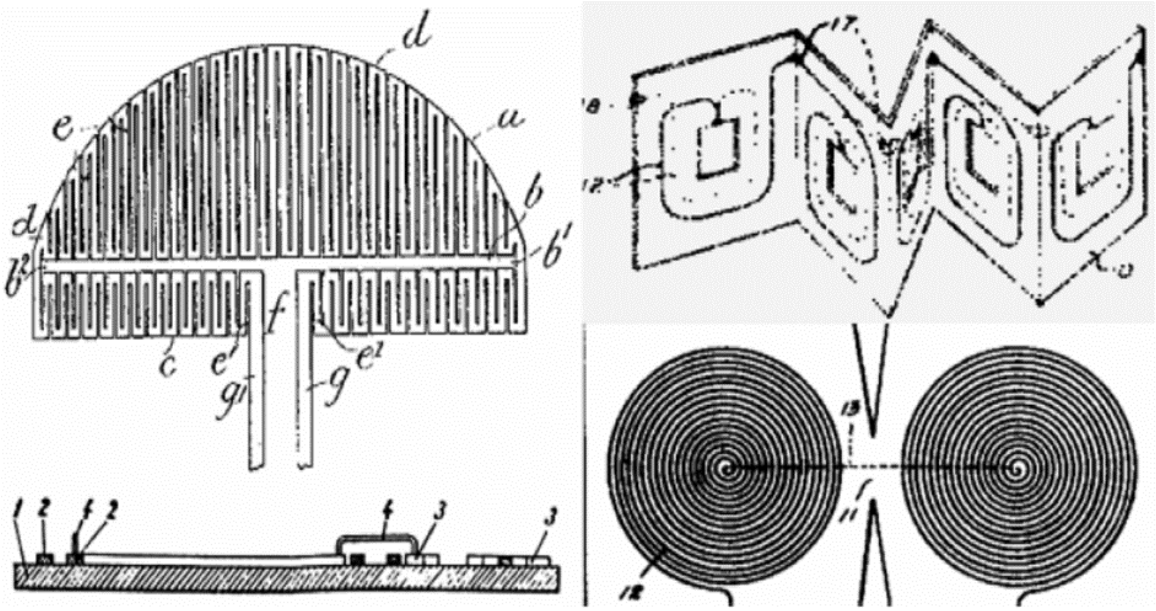

Figure 2: Flex patents from 1902-1903

interconnects that were developed in the first quarter in the "Age of Electronics" were flexible (Gilleo 2). Figure 2 shows diagrams of "old flex" technology from 1903-1925 that helped in pioneering modern principles used today (Gilleo 3).

The flex technology from the 1920's was way ahead of its time. For this technology to morph into what we know it as today though, technological revolutions, namely in solid-state electronics, would be required to allow flex to evolve into the technology we know so well today that allows for the interconnect, packaging, and circuitry technology of today (Gilleo 3).

1.2.2. Modern Flex

The highest density, lightest, and thinnest systems in the world of PCB's is flex circuitry (Gilleo 3). This flex technology spans a miraculously wide range of complexity making it useful in almost every product (Gilleo 3). Screen printed, and ink-jetted Polymer Thick Film flex circuits and keyboards are used in everything from computers to calculators and cell phones. The most low-cost processes use printed carbon ink on thin polyester film, however this methods performance is limited and does not always yield the best results. The international space station utilizes flex technology with giant circuits used for solar arrays (Gilleo 3). The arrays are connected with copper on polyimide, a specific version of DuPont's Kapton which was specially treated to resist solar wind damage (Gilleo 3). These arrays were folded up accordion style only to be unfolded high above the earth where they are still in use under the most extreme conditions (Gilleo 3). Not only is this technology greatly used in the aerospace industry, it is a critical component in medical electronics particularly in the field of bionics. There are several companies developing sight restoration technology using very thin and pliable interconnects. Figure 3 shows concepts developed by Second Sight that connect retinal sensors to electronic hardware.

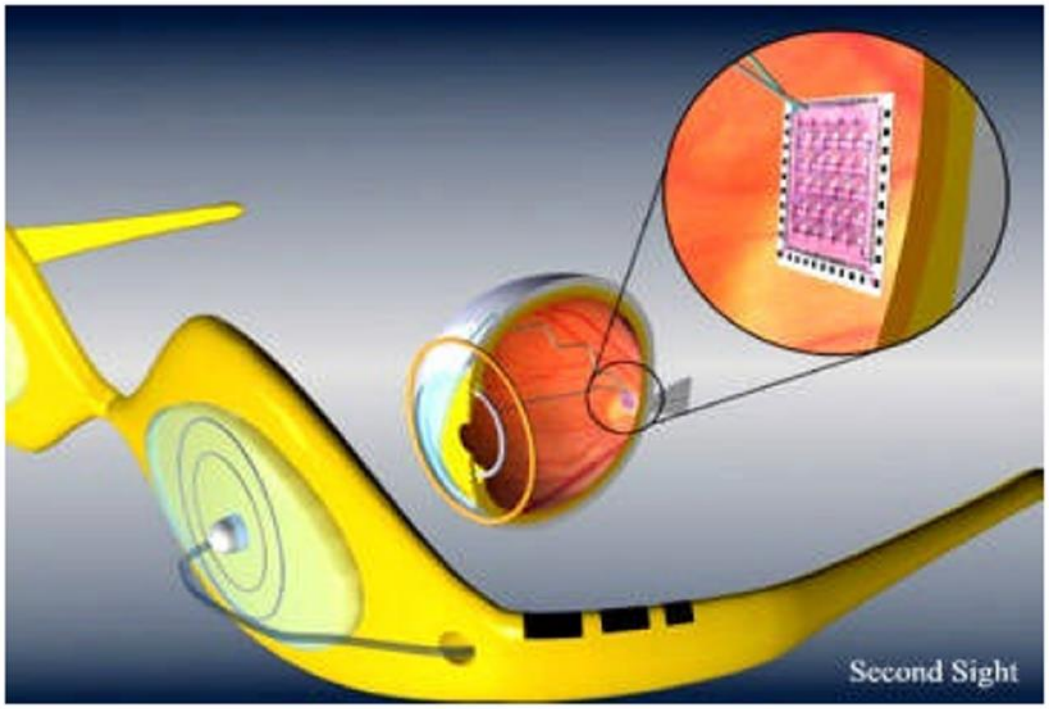

Figure 3: Second sight vision bionics concept

This technology is also prevalent in pacemakers, hearing aids, medical sensors, monitors, drug delivery systems and attachable electrodes (Gilleo 4). Figure 4 shows multiple medical devices that all utilize flex enabled products. The following products (not to scale) are (1) a PTF electrode, (2) 3M hearing aids, (3) pacemaker circuitry, (4) DNA analyzer, (5) wearable oxygen-sensing spectrophotometer made using PTF. When assembling the SMD's, conductive adhesives are used.

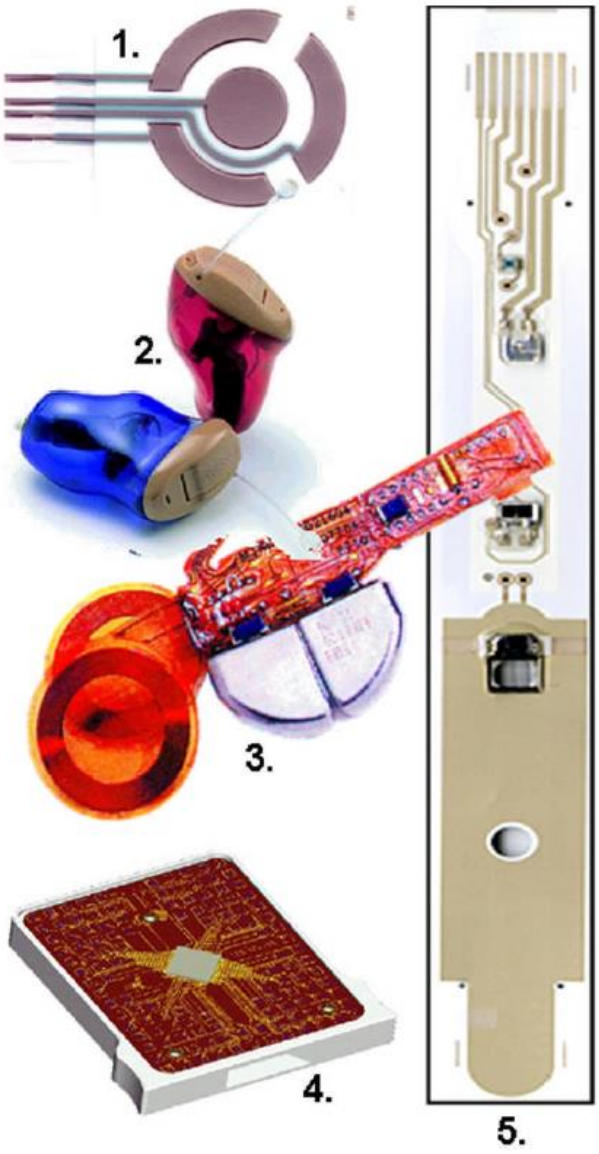

Figure 4: Medical devices utilizing FLEX circuitry

1.3 Past Research on Flexible Electronic Circuits and Sensors

The concept of printing electronics originated in the early 1990's. Francis Garnier, in 1994, created a field effect transistor from polymer materials using printing techniques (Garnier 1684). The device showed high current output while remaining insensitive to mechanical treatments such as bending and twisting (Garnier 1684). All organic devices such as conjugated polymers and oligomers were used as the

active layers in electronic devices such as field-effect transistors (FET's) and electroluminescent diodes (LED's). By further using organic compounds as the substrates or contact electrodes, "all organic" devices were developed for FET's and LED's showing a promising perspective of fabricating low-cost, large-area, flexible devices (Garnier 1684). Even though the term "all-organic" is used the reported structures still contained the gold source and drain electrodes in the FET's and rectifying calcium or magnesium electrodes in the LED's. This presents a potential source of mechanical and chemical instability with intefaces that cannot be considered to be fully flexible (Garnier 1684). The devices created by Garnier were fabricated solely using printing techniques and show the possibility of printing plastic electronics further advancing the field of flexible electronics (Garnier 1684). Garnier reported that the field-effect mobility that was calculated from transconductance (gm) in the linear regime from:

$$g_m = (\delta I_D / \delta V_D)_{V_D = cst} = (W/L) C_i \mu_{FET} V_D$$

where I_D is the drain current, V_g and V_D are the gate and drain voltages, respectively, C_i is the capacitance and cst is a constant. The value for μ_{FET} of $6x10^{-2}$ cm^2 V^{-1} s^{-1} is in excellent agreement with values obtained from devices made using conventional methods. The study also showed that mechanical operations on the device including rolling it up, bending, and twisting up to angles of 90˚ did not affect the electrical properties of the device (Garnier 1685). It was also noted that by lowering the insulating film thickness and increasing its dielectric constant would increase the capacitance of the device improving its response (Garnier 1685).

Screen printing of electronics was studied by Zhenan Bao in 1997 when he successfully screen printed a high-mobility plastic transistor (Bao 1299). By utilizing the purely additive method they reported that patterns could be made in a single step yielding traces as fine as 250 μm while significantly reducing time and cost associated with photolithography (Bao 1299). This research also concluded that their high-mobility plastic transistors field effect mobilities were very similar to those created on Si substrates with SiO2 gate dielectric layers (Bao 1300).

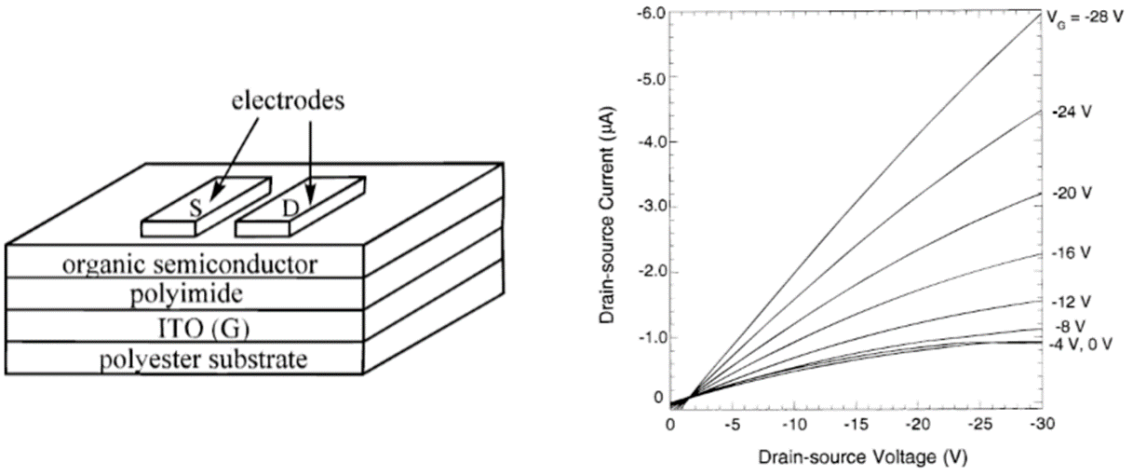

Figure 5: Structure of a printed plastic transistor, Current vs Voltage characteristics of the plastic transistor operated in accumulation mode at different gate voltages

Inkjet-printed circuits adequate for applications such as active matrix displays, and identification tags were demonstrated by H. Sirringhaus in the UK in 2000 (Sirringhaus 2123). It was reported that the performance of the inkjet printed, all polymer thin film transistor (TFT) circuits were comparable to all polymer TFT circuits created by the Philips group who utilized a 3-level photolithographic process (Sirringhaus 2126).

Force sensors are critical to a large range of different devices and systems.

Commercial force sensors are not often designed for specific system

requirements. This can result in the frequent use of sensors that are excessive in size, cost, and fragility. The ability to print these sensors for specific applications not only minimizes cost but provides force sensors without much lead time that are cost efficient and customized for their specific purpose (Xu 9). Force sensors convert applied forces by measuring displacement or strain of an internal element known as a flexure. When creating force sensors, there are generally 3 components. These components are the flexure, the transducer, and the packaging. The transducer converts the displacement to an electrical signal and the packaging helps protect the components and usually allows for mechanical connections to whatever system it will be integrated into. The flexure converts forces applied to the sensor along a specific direction into a displacement or strain that can be measured by the transducer (Xu 9). The sensitivity, accuracy, and directional response of a sensor are all determined by the mechanical properties, size, and shape of the flexure (Xu 9). Force sensors are usually comprised of flexures with a high stiffness which will produce small maximum displacements and small strains (Xu 9). Strain gauges and piezoelectric elements have good linearity and higher resonant frequencies and work as small strain transducers that are good for strains and displacements that aren't too large (Xu 9). The use of such small devices increases complexity and difficulty of assembly, while the small measured signals also require the use of sophisticated software and electronics to amplify the signal so that results can be obtained (Xu 9). Some materials used can display viscoelastic and hysteretic properties and are therefore not suitable for the creation of flexures. These undesirable sensor properties can be overcome by

selecting the right materials when looking to create flexures using printing processes (Xu 9). The pioneering of these methods to create electronic devices opened a whole new area of research to be conducted in the development and fabrication of sensors and electronics using flexible substrates and inks or inserts. New research and manufacturing techniques have begun to pave the way for flexible, wearable electronics. These flexible circuits and sensors are of great interests in the areas of soft robotics, human/machine interfaces, wearable electronics, custom sensors, and skin-mountable and wearable sensors. These new types of electronics require new and innovative processes, sometimes using materials not used in traditional electronics, to come up with working circuits or sensors that behave just as good if not better than their rigid counterparts. These new emerging techniques use some conventional processes in unconventional ways while also incorporating new methods and materials as well. A few of the processes that are used in the development of these devices includes lithography, planar printing, coating, microchannel molding, filling, and lamination.

Electronics and sensors can be very costly to develop, and these new processes aim to create low cost fabrication methods as well as produce multifunctional electronics over large areas. Other benefits of these developing technologies are the ability for companies and researchers to create individual, highly unique sensors built specifically for their purposes. By providing cost effective routes for processing multiple different electronic materials at temperatures that are compatible with polymer substrates, the possibilities for custom flexible sensors and electronics are growing rapidly.

These methods of printed electronics have allowed for the exploration of new avenues when it comes to material processing and sensor development allowing sensors to be created on non-planar surfaces which is not currently possible using conventional wafer-based fabrication techniques. These breakthroughs will help enable conformable sensitive electronic systems like electronic skins that can be wrapped around the body of a robot or prosthetics, as well as uses with human/machine interfacing. Another great benefit of these new emerging techniques is the ability to develop low-cost fabrication of electronics on much larger areas than the standard wafers that are currently available. This is apparent when looking at the development of devices and sensors such as large area printed pressure sensors, RFID tags, solar cells, LED's and transistors.

Sensors are defined as devices that detect or measure physical properties and record, indicate, or otherwise respond to the physical property that is measured. The use of sensors has grown rapidly with the development of micro-machinery and micro-controllers allowing these complex sensors to be used in such industries as manufacturing, aerospace, medicine, and robotics. Additive manufacturing processes are attractive for their ability to be started and stopped almost seamlessly, allowing for the incorporation of complimentary fabrication processes or the embedding of components and subcomponents that were manufactured using traditional processes (Xu 13). Currently there is much research being conducted in electronic sensors for force, hearing, optics, etc (Xu 20). The electronic and force sensing modules are 3D printed almost effortlessly and other sensors and flexible circuits can take advantage of this by integrating commercially available

components into 3D printed structures or conductive traces laid using AM methods (Xu 20). These 3D printed sensors combine multiple important technologies such as electronic device design and emerging printing technology in ways that lower costs while producing electronics that meet conventional expectations. One of the easiest and most promising methods for making sensors is using additive manufacturing technologies with conductive inks. Conductive inks can be made in several different ways. Among the most common are to incorporate carbon, conductive polymers, silver nano-particles, and liquid metals usually containing gallium.

1.4 Techniques

Traditional methods for printing electronics and sensors used methods like rubber stamping. This process includes the use of a patterned structure, which has pre-patterned designs cut out. The object which is coated with an ink or solution is then brought into contact with the substrate that the desired sensor will be applied to. Once the object with the structure is removed from the substrate, the functional inks or solutions only remain on the areas of the substrate where direct contact was made. Etching then occurs on the surface and the parts of the material that were not covered by the ink are removed.

The process shown below uses gold foils that are 20 nm thick, PDMS as the rubber stamp master and a solution capable of forming a self-assembled monolayer (SAM) as the “ink”, in this case hexadecanethiol (Rogers 100). In this process the inked rubber stamp contacts a thin sheet of gold for a few seconds. Less than a second is not enough and anything around 1 minute causes the ink to spread which ruins the resolution that can be attained when the stamp is only applied for a few seconds

(Rogers 20). Etching the printed structure removes the gold not protected by the printed SAM (Rogers 20). Then the SAM is removed using heat which exposes the bare gold and enables good electrical contact between the printed structures and layers of organic semiconductors cast on top of them.

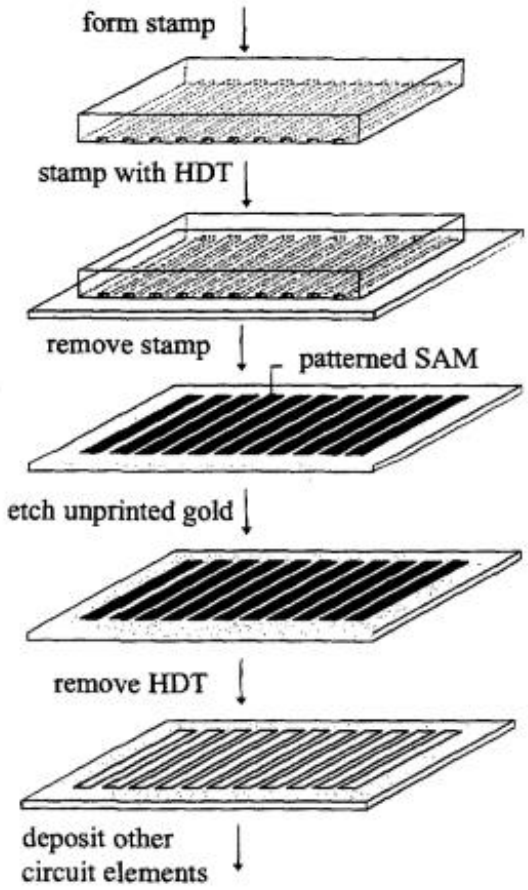

Figure 6: Steps involved in micro-contact printing

This type of process is called micro contact printing (Rogers 99). Contact printing processes involve physically contacting the patterned structures to the substrates where the sensors or traces will be deposited.

Another method of contact printing that has been used to create flexible electronics on absorbent and non-absorbent substrates, is called flexographic printing, shown

in figure 7 (Kahn 3174). Flexographic printing can use a wide variety of inks that are either water based, solvent based, or UV curable (Kahn 3174). Flexographic printing is an example of convex direct printing done by using a flexible plate mounted on a printing cylinder (Kahn 3174). The convex reliefs are formed on flexible plates that were originally made of natural rubber, then synthetic rubber, and are now mainly made using photopolymers (Khan 3174). In flexographic printing, proper ink transfer can only occur when there is a slight pressure between the plate and pressure cylinders (Kahn 3174). As the substrate is fed between the plate and impression cylinders, ink is transferred to the plate cylinder by an anilox roller (Izdebska 186). The anilox roller is a roller that has millions of microscopic channels called cells which roll through a liquid ink and provide a measured amount of ink to the printing plate while excess ink is removed by a so-called doctor blade (Izdebska 183). Other forms of contact-based printing technologies are gravure printing, gravure-offset printing, and R2R (roll-to-roll) printing.

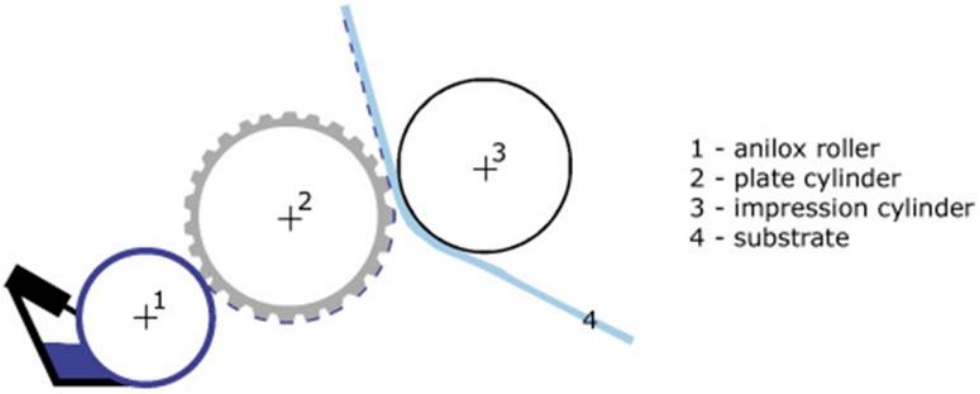

Figure 7: Flexographic printing unit

Some non-contact processes involve solutions being dispensed through openings or nozzles and the structures are defined by moving the extrusion head or the stage

of the printing machine in pre-programmed patterns (Muth 6307). The method works exactly like the fused deposition modeling process used in additive manufacturing. The only difference is in how many layers are used. FDM printing usually uses hundreds of layers of material and works by the extrusion material being heated through the dispensing nozzle until it reaches its glass transition temperature. The difference with using inks and pastes is that usually the head doing the printing is in the form of a syringe and the heat application if used at all comes after the inks or solutions have been deposited allowing for the sintering of the particles in the solutions or inks. The method that drives the material out of the syringe can be seen in figure 8.

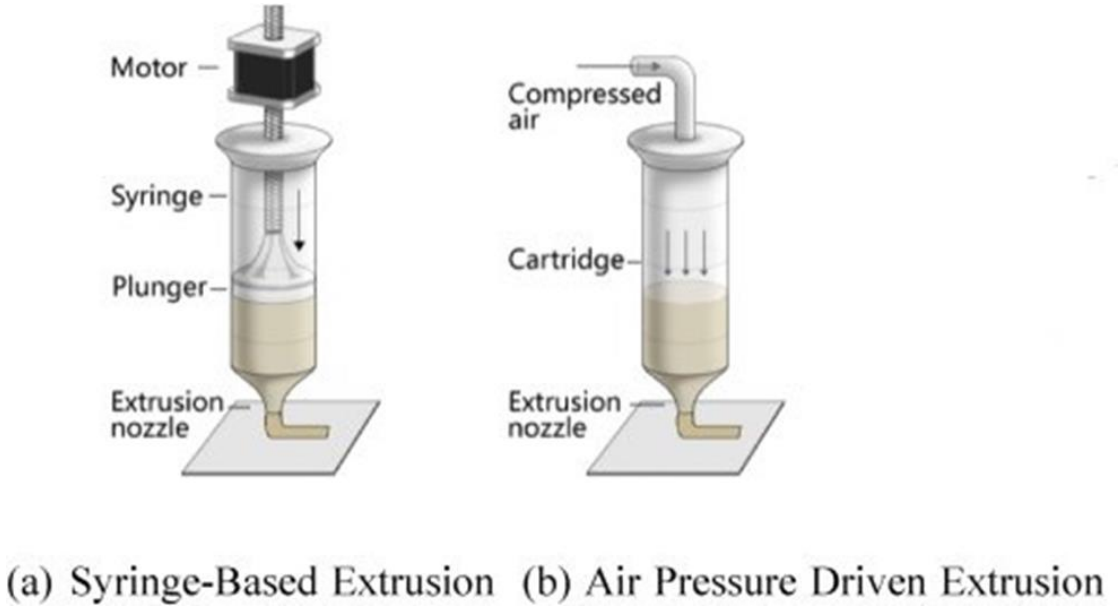

Figure 8: Two different drivers for syringe deposition systems

Other non-contact processes include inkjet printing. When looking at the inkjet printing methods, ink is either dispensed through the nozzle by one of two primary types of printhead technologies: piezo and thermal. Piezo print heads use

microscopic piezoelectric elements behind the print nozzles. Piezo electric devices expand and contract when electrical charges are applied to them. By controlling the amount of electrical charge, the piezo crystals or ceramics receive, the amount of deformation can be controlled leading to tiny droplets of ink being ejected from the nozzle falling on the substrate below. The thermal heads work by electrifying microscopic resistors behind the print nozzle, which creates intense heat that vaporizes the ink causing it to create a bubble that expands rapidly causing the ink to explode onto the substrate. The process in both thermal and piezo print heads happens multiple times until the whole image or traces are complete.

Piezo print heads are the preferred method to use over thermal because of sintering that may occur before the material is deposited onto the substrate. Both of these methods for actuating an inkjet printer head can be seen in figure 9. Piezo print heads offer precise and variable droplet sizes while thermal methods only offer large or small droplet sizes. Ink options for use in piezo print heads are also more abundant since they will not be affected by heat like they would if using a thermal print head. The downsides to piezo print heads are their higher costs and fewer print heads per printer, however the piezo print heads can run longer due to cooler temperature while printing and not needing to be replaces as often as thermal print heads.

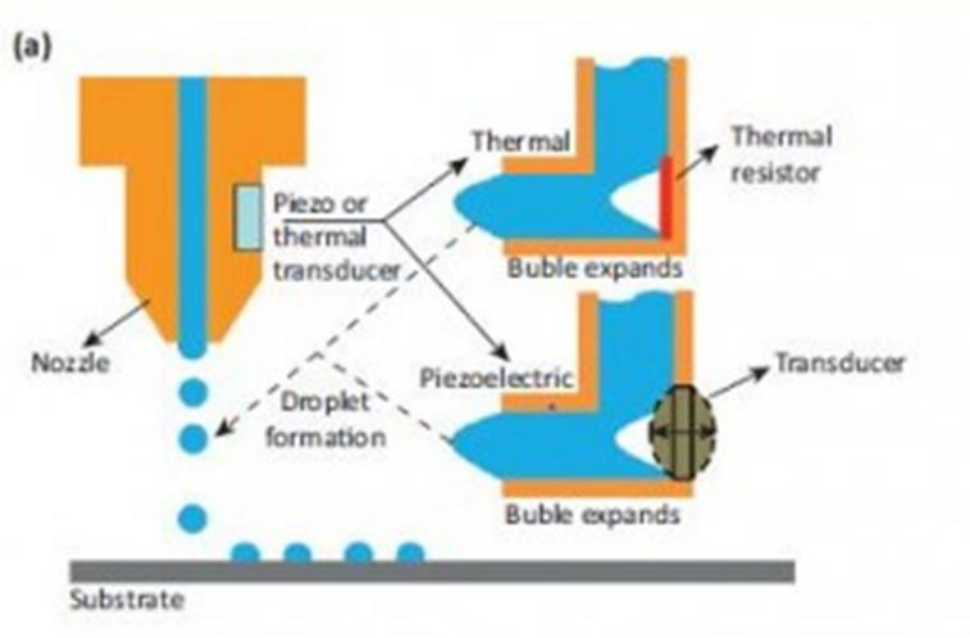

Figure 9: Piezo and thermal activated inkjet printer mechanisms

Screen printing of electrical circuits and sensors is another viable option that has been researched for flexible circuits. Screen printing is a type of stencil process that utilizes, closed non-image areas and open image areas. The stencils are usually made using a light sensitive emulsion that is photographically imaged so the printing areas are washed away while the non-image areas are left intact. The stencil is created using a fine fabric which holds parts of the designs in place. When an image is ready to be printed, the screen/mask is laid down on top of the substrate where electrical traces or sensors will be left. Ink is forced through the screen by use of a squeegee that covers the whole pattern so that no spots are missed which can be seen in figure 10. The screen is then removed revealing a circuit or sensor which is also shown on the right in figure 10.

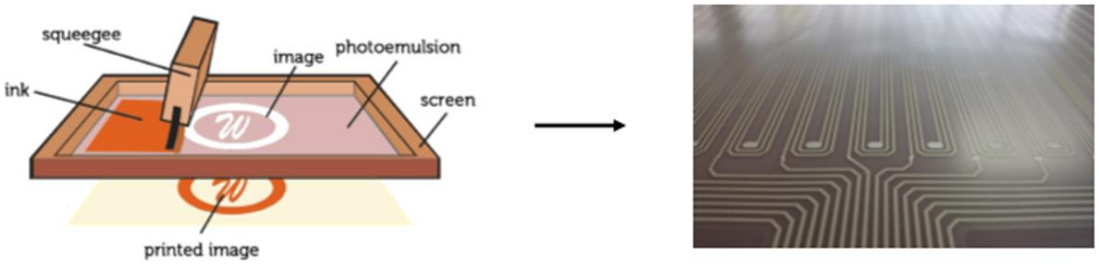

Figure 10: Screen Printing process, Traces made using the screen printng process

Non-contact printing techniques have been more sought after due to their simplicity, affordability, reduced material wasting, high pattern resolution and easy controllability by adjusting only a few process parameters. Other advances in 3D printing have brought about a way of creating sensors with multifarious purposes and advantages. These AM approaches offer a new scope for sensor fabrication.

1.5 Problem Statement

There is a need for a myriad of different sensors created using non-specialized equipment and materials that are easily obtainable. These sensors require the use of materials that will give as close to a response as possible of commercially available sensors created using traditional manufacturing methods. The goal of this research is to design and develop sensors using these non-conventional methods and materials that when characterized give meaningful and useful results just like the non-customizable and expensive commercially available sensors.

Information gathered from the history and research sections above will be applied while designing and developing different sensors. The next chapter shows the reasons behind the specific designs as well as the motivations used in their creation.

CHAPTER 2

DEVELOPMENT OF DIFFERENT SENSORS

The sensors and flexible circuits proposed here all follow simple designs using methods mentioned in the previous sections of this paper. The designs were inspired by existing flexible circuits and sensors. Using non-conventional methods for electronic component fabrication and easily obtainable materials, sensors were made and characterized to show how feasible it is to create low cost sensors using non-specialized equipment. The following methods were used to create the sensors that are studied in this document are, foil-based methods, screen printing, planar printing using the Hyrel system 30, and pressure sensors made using piezoresistive materials. Piezoresistive pressure sensors are one of the very first MEMS technology products (Measurement Specialties 1). These types of products are widely used in biomedical applications, automotive industries, aerospace industries, and household appliances. The sensing material in piezoresistive pressure sensors is composed of a diaphragm that is traditionally built on a silicone substrate (Measurement Specialties 12). However, the purpose of this research is to develop these sensors using non-traditional methods. Therefore, silicone substrates will not be used in the manufacturing of the sensors created for this research. The pressure sensors still perform in the same way that traditional sensors do. The way the sensors work by mechanical manipulation of the diaphragm which causes deformation in the crystal lattice structure of the diaphragm due to the mechanical deformation. This deformation causes a change in the band structure of the piezoresistors that are placed on the diaphragm. This causes a change in the resistivity of the material which either causes the resistance to increase or decrease depending on the orientation of the resistors (Measurement Specialties 2). The physical causes of piezoresistivity are related to changes of relative dimensions

because the resistance is related to the length and local cross-sectional area of the material. This relationship can be attained from the following three equations (Liu 4):

$$R = \rho \frac{l}{A} \tag{1}$$

$$dR = \frac{\rho}{A} dL + \frac{L}{A} d\rho - \frac{\rho L}{A^2} dA \tag{2}$$

$$\frac{dR}{R} = \frac{dL}{L} + \frac{d\rho}{\rho} - \frac{dA}{A} \tag{3}$$

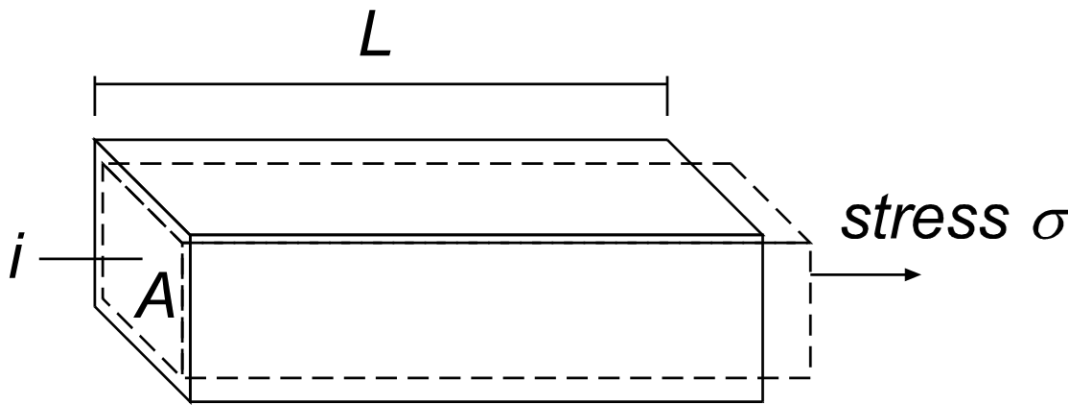

Figure 11: Change of relative dimensions as resistance is related to length and cross-sectional area (local)

In the research conducted in previous sections, electrical conductivity and resistivity has been shown to change with stresses and strains that deform the crystal lattice structure. The strain is the cause for the shape of energy bands curves changing which leads to the change in effective mass. This change in effective mass causes changes in the electrical conductivity (Liu 4). Figure 12 below shows a graph of the crystal bandgap structure and the derived equations are labelled 4 and 5 below (Liu 5).

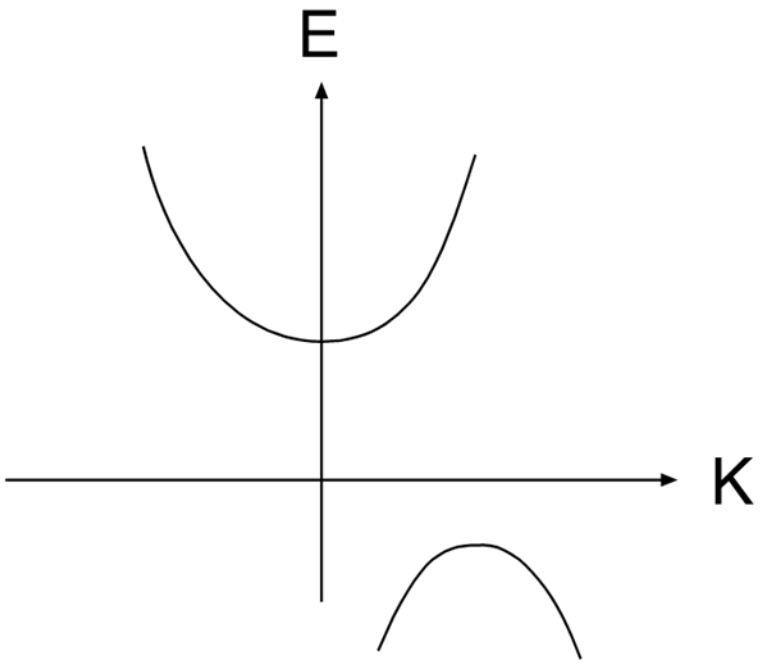

Figure 12: Crystal bandgap structure

$$m^* = \frac{h^2}{d^2E/dk^2} \tag{4}$$

$$\sigma = \frac{q\bar{t}}{m^*} \tag{5}$$

Gauge factors for piezoresistors are identified by the symbol G. The gauge factor determines the amplification factor between strain and resistance change. Gauge factor can be found utilizing the following equations which describe piezoresistivity (Liu 6):

$$\frac{\Delta R}{R} = G * \frac{\Delta L}{L} \tag{6}$$

$$G = \frac{\frac{\Delta R}{R}}{\frac{\Delta l}{l}} = \frac{\Delta R}{\varepsilon} \tag{7}$$

Table 1 shows common ranges of gauge factors for different materials (Liu 6).

Table 1: Guage factors of common materials

Material	Gauge factor
Metal foil	1-5
Semiconductor (crystal)	80-150
Diffused semiconductor	10-200

2.1 Design of Velostat sensors

Using facts gathered from the information above and other documents, one way of developing a low-cost pressure sensor using easily required materials can be created by using Velostat or Linqstat. Both are manufacturer names for a piezoresistive material. The sensitivity of piezo film as a receiver of mechanical work input is awesome (Measurement Specialties 2). The film behaves like a dynamic strain gauge, but it does not require any external power and is able to generate signals greater than those seen in conventional foil gauges even after amplification (Measurement Specialties 5). This sensitivity is largely due to the format of the piezo film material (Measurement Specialties 5). Due to the low thickness of the film, the cross-sectional area is very small, therefore relatively small longitudinal forces create very large stresses within the material (Measurement Specialties 5). This becomes the main aspect used to enhance the sensitivity parallel to the machine axis (Measurement Specialties 5). When the film is compressed the forces are converted into longitudinal extensive forces with much larger magnitudes (Measurement Specialties 5). A benefit of using these film transducers is their ability to cover a much larger are than conventional strain gauges.

The energy output from the force sensors is proportional to the volume of the film that is stressed (Measurement Specialties 6). Choosing a film thickness may be

based on optimizing the electrical signal or for making sensors with better mechanical strength (Measurement Specialties 6). Thicker film sizes will generate higher voltages but form smaller capacitances (Measurement Specialties 6). Areas of the sensor that are not undergoing stress act as a capacitive load on the "active" area, when creating sensors using these films the sensor should be designed so that areas that will not undergo stress are minimized (Measurement Specialties 6).

To create the sensors a single piece of Velostat is sandwiched between two conductive pads. Due to its wide range of resistance change, this material is great for use in pressure and bend sensors. Once the Velostat is sandwiched between the two conductive layers, lead wires and be soldered to the conductive pads so that the sensor can be hooked up to devices like microcontrollers or other types of low cost pre-made circuits that help amplify signals for sensor reading. Figure 13 shows the simple sandwich construction used to create the Velostat pressure sensors.

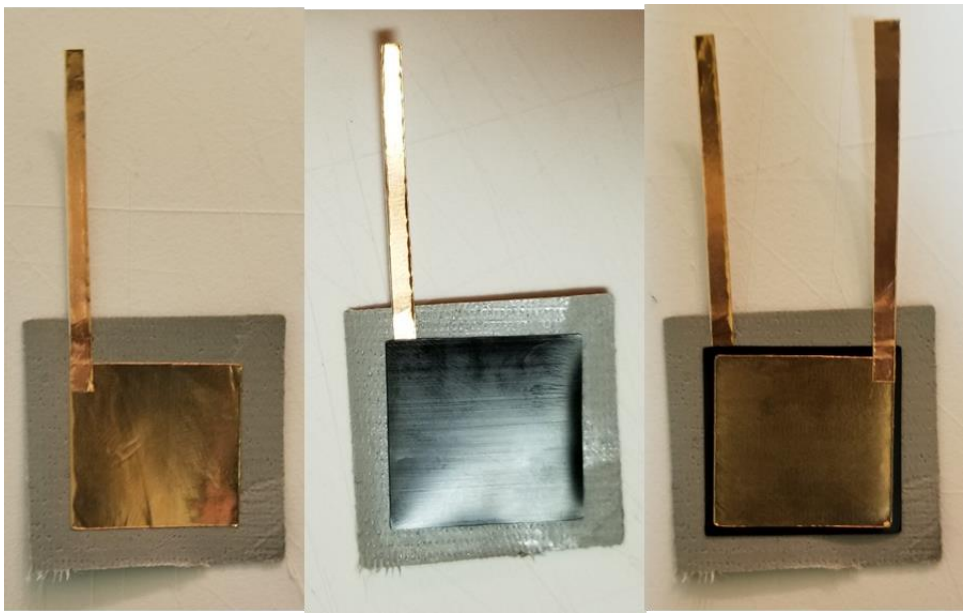

Figure 13: Sandwich construction of velostat sensors, first layer of copper foil, velostat square placed on top of foil, final copper foil square to sandwich velostat

To protect the packaging, a thick duct tape called Gorilla tape was used. This thick adhesive material was chosen for its durability and flexibility. Since one side is adhesive, it played a critical role in keeping the sandwiched pieces of conductive layers and piezoresistive Velostat in place. It also provided a way to guarantee contact of all the sandwiched components which plays an important part in the sensitivity and response of the sensor. Instead of using wire leads from the sensor, copper tape containing conductive adhesive was used to minimize the thickness of the package and to prevent any wires poking through the sandwiched layers which would have an effect on the sensors response. The copper tape was cut into 1" squares and was positioned in the center of the duct tape substrate. The adhesive was then taken off of the copper square and a 1.25" cut sheet of Velostat was placed on top so that it would stick to the adhesive of the copper tape and the adhesive of the duct tape substrate. Another 1" copper conductive sheet was placed on top of the Velostat with another thin copper tape lead coming off of it. Once the conductive layers of copper and the Velostat were stacked in the correct configuration the last layer of duct tape that would act as the packaging for the entire sensor was placed on top effectively securing the layers in the sensors position as well as protecting all the inner components from any damage that may come due to placing weights and other heavy objects on the sensor during the testing phases. The final product can be seen in figure 14.

Figure 14: Complete packaged velostat sensor

2.2 Design of Force Sensing Resistors (FSR's)

FSR's are resistive sensors that respond to forces applied to the sensor by varying the resistance. The sensors resistance decreases as force increases on the sensing area. Generally, there are 2 types of FSR's, ShuntMode and ThruMode (Sensitronics 3). Both types utilize two terminals as well as two layers and both operate using the same working principle (Sensitronics 3) The major difference between the two is the force vs resistance response curves which are usually only looked at when considering different design applications (Sensitronics 3). ThruMode FSR's are made by placing a solid semiconductive element on top of a solid conductive area, like the sensors seen above the copper later was a single sheet of adhesive copper (Sensitronics 4). The solid conductor from each layer runs to only one output terminal (Sensitronics 4). By utilizing two layers any excitation current passes through one layer and then into the other layer which is why it is designated as a through type sensor (Sensitronics 4).

ShuntMode FSR's are among the more common method of construction types (Sensitonics 3). In ShuntMode the top layer is a solid area made from a

semiconductor just like in the ThruMode sensors, this later gets deposited on a flexible substrate (Sensitronics 3). The bottom layer however, is made up of conductive traces also on a flexible substrate. These traces are arranged into a set of interdigitating fingers (Sensitronics 3). When force is applied to the sensor on the sensor area, the top layer shunts the interdigitated fingers on the bottom layer which causes the resistance to vary across the output terminals (Sensitronics 3). The force sensing resistors are characterized using resistance vs force curves where the sensors resistance change is plotted as a function of the force applied (Sensitronics 5). The curves vary depending on the design of the sensor such as finger width, length, and spacing between traces (Sensitronics 5). Figure 15 shows four different FSR's. The sensors pictured were made using adhesive copper tape with a conductive adhesive. The tape was placed into a vinyl cutter that had images taken from drawing exchange format (.dxf) files generated using CAD software such as SolidWorks to ensure that the correct sizes remain that were designed for remain intact across different programs that are used for vector based drawing which is what vinyl cutters use as input to trace the selected contours onto a surface using a tiny razorblade. The specific vinyl cutter used is a Roland GX-400 with a 39" wide work area and an accuracy of 0.0124mm.

Figure 15: Interdigitated fingers and traces made from copper foil before velostat is placed on top of the traces, 1mm, 3mm, 5mm, and 7mm respectively

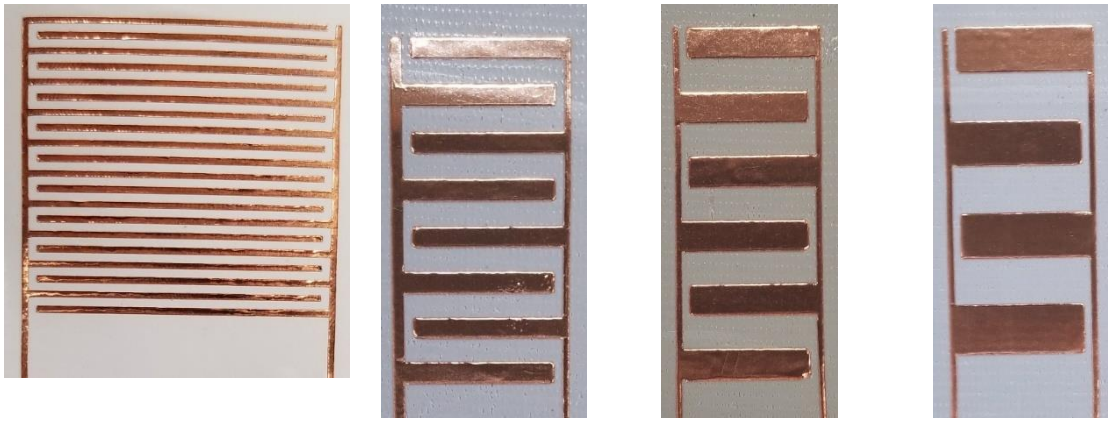

Force sensing resistors are primarily characterized by a force vs resistance curve where the sensor resistance is plotted as a function of the applied force. The curves can generally be approximated by some function of the form $y = ax^{-b}$ (Sensitronics 5). The following figures show a typical plot of a single zone FSR. As can be seen from the graph in figure 16 the relationship is non-linear (Sensitronics 6). When the same data is plotted using logarithmic scales for the x and y axes, the result becomes near linear as seen in figure 17 (Sensitronics 6).

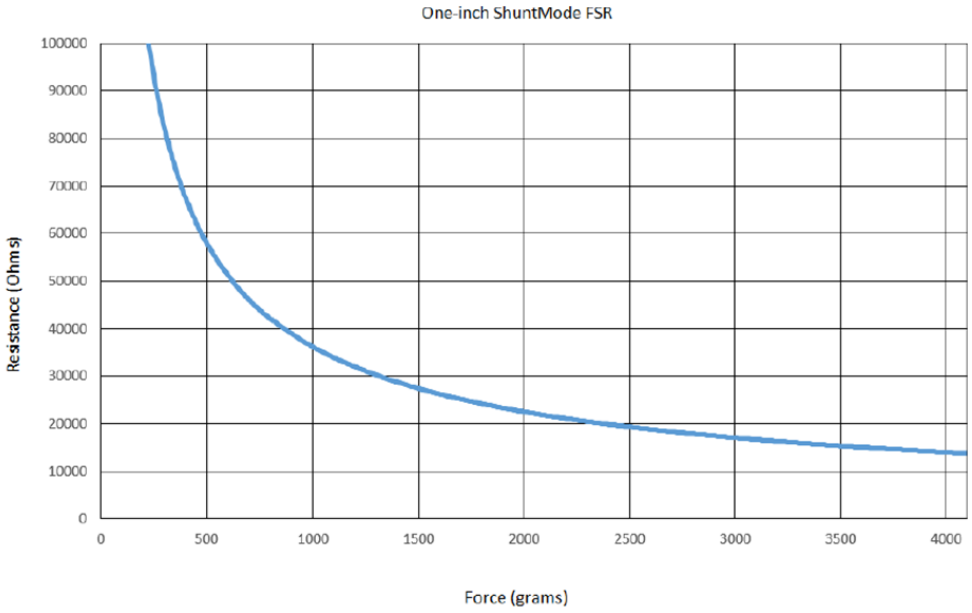

Figure 16: FSR example characteristic curve

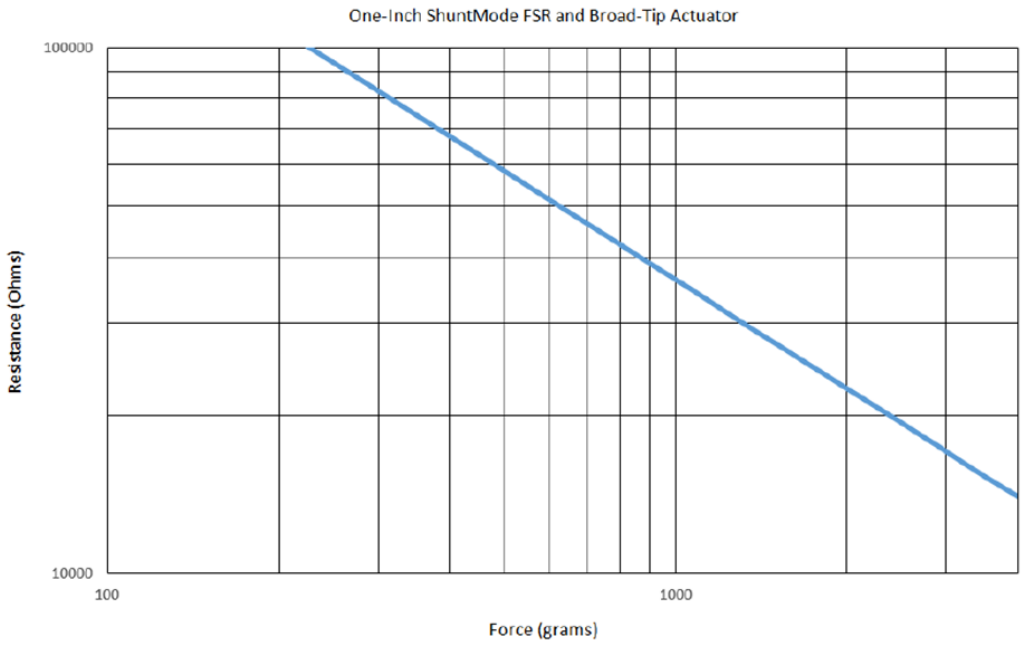

Figure 17: Example FSR curve plotted on a logarithmic scale

There are generally 3 different configurations to look at when grouping these types of sensors (Sensitronics 4). In this paper, single zone and discrete arrays are made and tested. Single sensors were designed and tested first before an array of sensors in the form of a pressure sensing mat were constructed. The four different sensors shown in figure 15, were created and tested so that a good sensor design candidate could be chosen for the sensor array mat. As shown in the testing and results section below the 1mm traces and spacing design was the most sensitive and gave the most repeatable results. Using the best responding sensors, made of 1mm traces, a sensor array mat was developed for testing. In a discrete matrix array, a collection of any number of single-zone sensors are placed on a single substrate. The two terminals of each sensor element can be combined into one trace or they can be traced out individually. The mat made utilizing the discrete matrix array created uses individual traces for each element. This was done to reduce complexity while making sure that all connected elements displayed continuity without interfering

with any other traces or elements. Figure 18 shows the mat with the interdigitated fingers made from copper foil with traces and spacing of 1mm.

Figure 18: 1mm spaced interdigitated fingers and traces of FSR sensor array

Once fabrication of the mat was completed and tested, the results below show that the sensors behave like commercially available FSR's and were built at much larger sizes and for much less than the commercially available FSR's produced by SingleTact. SingleTact makes ultra-thin capacitive miniature force sensors. SingleTact makes use of the same design and materials to create their sensors that can be purchased for $50 dollars uncalibrated and $75 dollars calibrated (SingleTact Website). Total cost of one of the sensors made in the lab is a little bit hard to determine since multiple sensors can be created from the materials bought. Total cost for materials to make many sensors only costs around $25. Using only $25 at least 50 different styles of sensors were created before the final 1mm trace and spacing design was utilized and tested, and a sufficient amount of material to continue producing sensors was left. SingleTact notes on their website that calibration does not affect the repeatability, sensitivity, hysteresis, drift, or response time (SingleTact Website). Sensors that were created in the lab were not individually calibrated and matched for use with only one board such as the SingleTact sensors, meaning they can be swapped between multiple electronic devices which cannot be done with the SingleTact sensors if you would like them to remain calibrated. Another downside to the calibrated SingleTact sensors is that if the sensor itself is damaged, the electronics that cost an extra $25 dollars are essentially useless and cannot be used with other sensors since they are calibrated for one individual sensor and that calibration is flashed into the electronic board that comes with the sensor (SingleTact Website). This issue is not seen with the sensors that were created in the lab. This is possible because of the use of a very

simple but very fundamental circuit known as a voltage divider. Many sensors that are produced are simple resistive devices and the sensor created in the lab for these experiments is no exception. Since voltage is much easier to measure for microcontrollers as opposed to a change in resistance, setting up a voltage divider circuit is not only simple but makes the reading of the sensor output much easier to read using a simple microcontroller and gets rid of extra steps such as those seen when using SingleTact sensors. Voltage dividers work by applying a voltage source across two resistors configured in series as seen in figure 19 (Sparkfun Website).

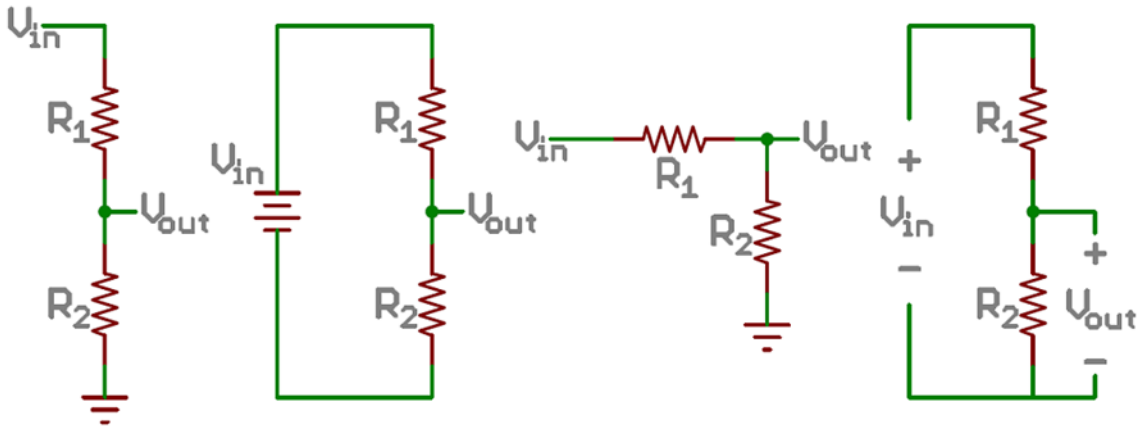

Figure 19: Common voltage divider circuits

The resistor closest to the input voltage, V_{in}, is designated as R_1 while the resistor closest to ground, is R_2. The Voltage drop across R_2 is the voltage out, V_{out}, that divides the voltage to a fraction of the input voltage. The general equation of V_{out} can be found using the following equation (Sparkfun Website):

$$V_{out} = V_{in} \cdot \frac{R_2}{R_1 + R_2} \tag{8}$$

The voltage divider equation assumes that the 3 values above, V_{in}, R_1, and R_2, are all known. By knowing the resistances and how much voltage is being applied,

the voltage out, V_{out}, can be found (Sparkfun Website). This technique is used for sensor characterization and is discussed further in the testing and results section.

2.3 Design of Foil Strain Guages

Strain gauges have been created using copper foils that are cut into very thin traces. These thin metal traces or foils can be integrated into electrical circuits to measure strain (Gostick 110). Strain gauges have been created out of thin metal strips since not only mechanical properties, but electrical properties change as the metal deforms (Gostick 109). The resistivity of certain metals is an intrinsic property that is independent of size and shape of the metal object which can be seen in figure 20 (Gostick 109). The resistance of the metal, however, does depend on the shape. This can be seen by Pouillet's law which states that if you increase the strip of material to two times its initial thickness, the strip will carry twice the current (Gostick 109).

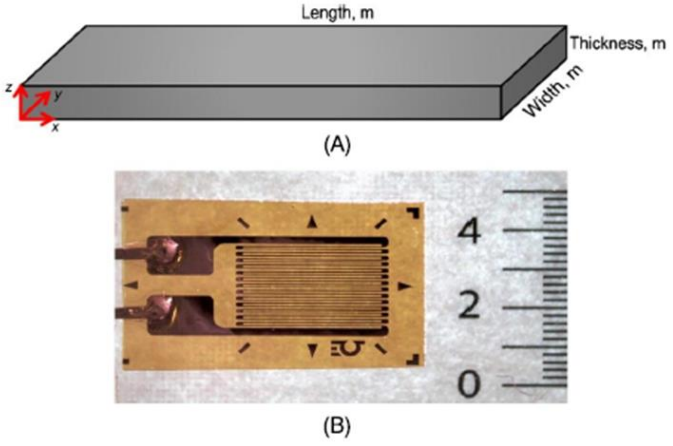

Figure 20: A) Electrical resistance changes as the object is elongated, B) actual strain gauges are more complex. Serpentine patterns increase resistance by elongating the trace and strain is seen at each inflection. Ruler has units of mm.

Equation 9 shows the same resistance equation used in the above section (Gostick 110):

$$R = \frac{\rho L}{X_A} \tag{9}$$

Where L is the objects length in the direction of current flow, and X_A is the cross-sectional area. Another thing can be deduced from the above equation, is that as the strip stretches, it increases in length but decreases in cross-sectional area which both cause a change in resistance (Gostick 110). The change in the cross-sectional area X_A depends on Poisson's ratio ν, which is the ratio of the strain perpendicular and parallel to the direction of deformation. When looking at cases using round wires with an unrestrained radius r_0, Poisson's ratio, $\nu = \frac{\frac{\Delta r}{r_0}}{\frac{\Delta L}{L_0}}$. For small amounts of strain, the density and therefore the volume remain constant (Gostick 110).

Using these above properties, it can be seen that metal bars would make poor sensors (Gostick 110). This is due to the fact that small dimensional changes yield equally small changes in the structures resistance (Gostick 110). Commercial strain gauges are coiled which increases the electron conduction path length making the sensors more sensitive. By adding more loops to the coils, the sensitivity of the gauge is increased (Gostick 110). This effect can also be seen when decreasing the thickness of the material which is another reason other than being flexible that thin copper foil was used. Copper Tape consisting of a conductive adhesive was placed on top of sheets of vinyl. The vinyl sheet was then loaded into a vinyl cutter that is accurate down to 12.4 μm.

After the foil was loaded into the machine a vector file created from the desired pattern of the gauge to be created was loaded into the software and the cutting process began. Once the material was fully cut the sheet of copper tape was unloaded. With the pattern cut onto the foil post processing done by hand was required to remove the unwanted material. Figure 21 shows the process from before cutting, during material removal, and final product.

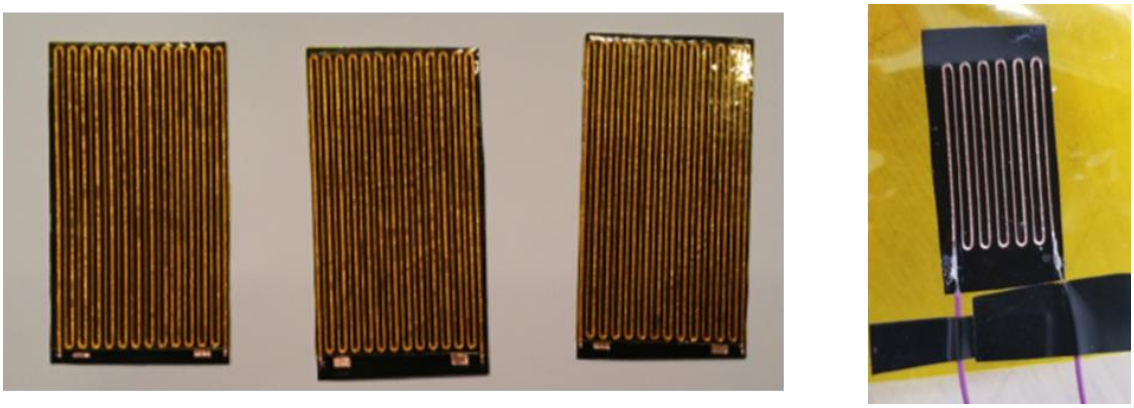

Figure 21: Foil gauges on Kapton, foil before beng enclosed with Kapton

The foil strain gauges were covered with a layer of Kapton to protect them from any damage and solder pads were left where wire leads were to be connected so that adjusting resistors could be placed on the sensor for reading in a Wheatstone bridge. Other systems not requiring the use of a wheatsone bridge are the use of a strain gauge module which can be used with many micro-controllers. The strain gauge module used is produced by Elecrow and can be seen in figure 22 along with the wireless module assembly. This module is pictured below with its commercially available strain gauge. The printed foil sensors that were created were soldered to the leads of this module after the existing sensor was removed. The device could also be attached to a micro-controller with Bluetooth

capabilities so that strain information is able to be sent wirelessly to handheld or computer devices.

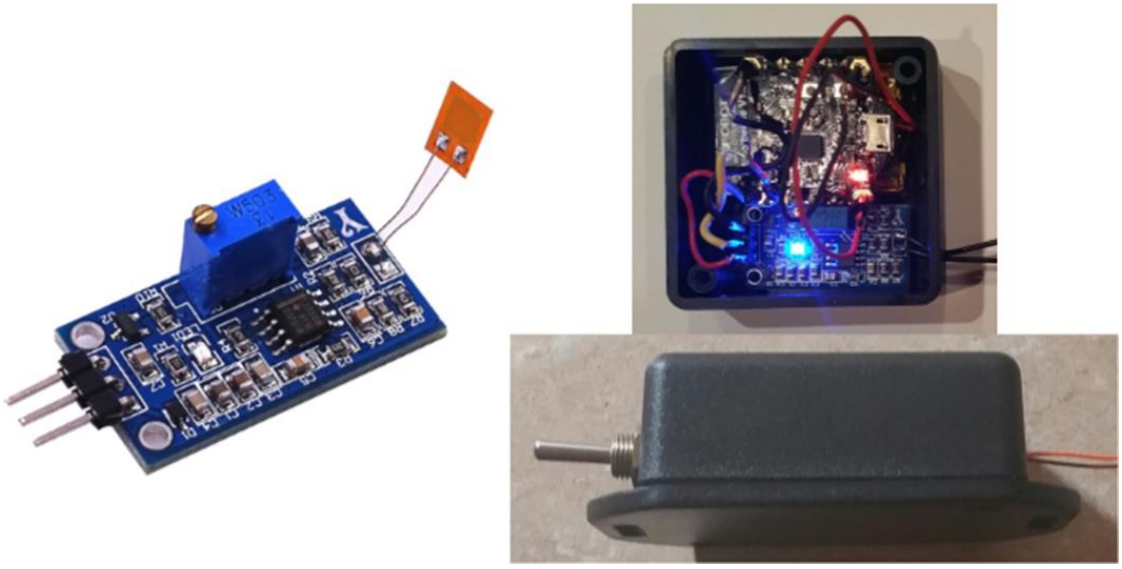

Figure 22: Strain module, Strain module and Bluno connected and transmitting strain information, transportable wireless strain gauge data transmitter.

The wireless module would be able to be mounted close to where the strain gauge would be glued down and would be able to transmit data collected using an internal battery to a nearby computer. This means that a unit that receives and records data would be able to be stored on a plane and the plane would have multiple sensors attached to different parts that needed to be monitored. Each sensor module would capture the strain on parts during the flight. The development of these sensors would let maintenance be done on plane parts and allow for parts to be swapped out as needed instead of being replaced after only so many hours.

2.4 Design of Screen Printed Sensors

Using a serpentine pattern to maximize length, therefore increasing resistance, strain gauge masks were created using multiple materials. Masks were fabricated on a vinyl cutter and a laser cutter with traces varying from 500 microns to 1 mm. The total length of the traces varied between 120mm and 130mm. Since the traces are long and thin, parts of the mask did not stay evenly spaced when the masks were placed on the substrate. This would result in traces and sensors that were not repeatable.

To combat this a thin layer of adhesive was laid down before the mask was laid which allowed the mask parts to remain exactly where they were laid or even to be adjusted so that the spacing between traces remained the same. Once the mask was laid and positioning was verified, a conductive ink was applied at one end of the pattern and a dual edged squeegee was used to spread the ink across the surface of the mask filling all the open portions with a thin layer of conductive ink measuring about 500μm thick. The paint used is a water based, water soluble electrically conductive paint (Bare Conductive Website). The data sheet for the paint states a typical sheet resistance of 55 Ω/sq while for screen printing this sheet resistance drops to 32 Ω/sq [Bare Conductive]. After the paint was laid onto the mask and substrate two different methods utilized to elicit the best results. In the first method the mask was removed directly after the paint had been spread on the mask allowing no time for the paint to dry while the second method allowed the paint to fully dry before removing the mask. Allowing the paint to dry was done to test the efficiency of using screen printing techniques since pulling the mask directly after pant was applied sometimes yielded muddy traces or traces that were obstructed due to parts

of the mask hitting the wet paint as the mask was removed. Figure 23 shows the different results obtained from both methods where the image on the left shows traces made when the mask was removed directly after paint was applied and the image on the right shows strain gauges that were allowed to dry before the mask was removed.

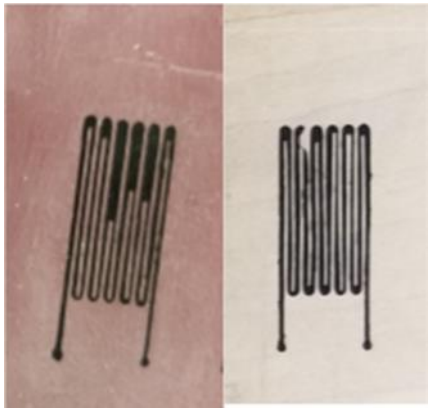

Figure 23: Some attempts at recreating a screen printing process

2.5 Design of Sensors using planar printing and direct writing methods

Planar printing and direct writing techniques are highly valued for their extrusion of ink filaments either in- or out-of plane with great accuracy. The process is a 1-3D printing technique which enables the deposition of features ranging from simple traces to complex structures through fine nozzles ranging in size from ~0.1-250 μm. Either the stage on which the material is deposited, the deposition heads, or a combination of both movements ensure that models made using CAD softwares can be implemented into the software and then directly written onto the substrate. The machine used for the fabrication of the printed strain gauges tested in this thesis is the Hyrel System 30M. The bed contains a heating element that heats to 90 C which will be turned on as the ink is deposited and will remain on after all the ink

has been deposited to allow for the sintering of particles in the ink. The ink used was obtained from Chem^3 Jettable Solutions^{TM}. Traces were also made using electric paint from Bare Conductive that was used to try and screen print strain gauges earlier in this paper. The ethanol-based silver nano-particle ink from Chem^3, has the same conductivity as bulk silver after it has been sintered. The silver ink can be applied to many different types of surfaces including Kapton, FR4 (PCB board), paper, polyester, and ABS, and also has a low sintering temperature of 80 C which makes this ink suitable for deposition onto flexible electronics and biomedical applications. This particular ink is usually used in ink-jet printers and can be used in printers utilizing either thermal or piezo actuated print heads. Due to the nature of the Hyrel System 30M and its capabilities, this ink will work well using Hyrel's syringe delivery system (SDS) heads. The SDS modular head created by Hyrel has been touted as being ideal for cost effective 3D printing aplications in biological, mechanical, medical, and electronic fields (Hyrel Website). The SDS extruders allow for the printing of material directly from syringes that can be easily filled with different materials and be swapped out or stored when not in use (Hyrel Website).

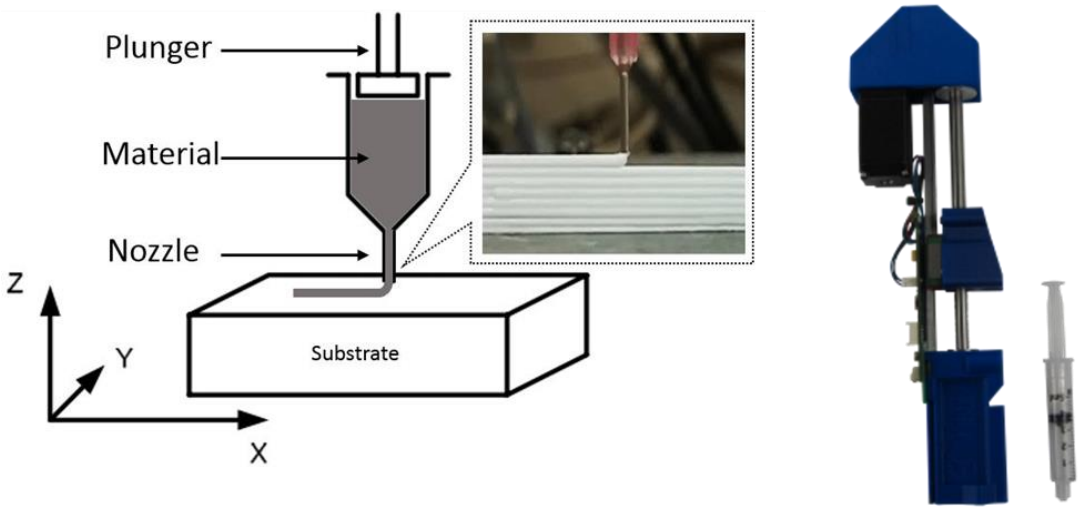

Traces for circuits and sensors were developed in SolidWorks. Once the traces have been designed they are saved as DXF files and imported into a program called Repetrel which is the software that runs the Hyrel System 30. Repetrel has its own slicing feature in which you can enter all parameters ranging from nozzle size to extrusion rate and print speed. The sensors created were printed on Kapton, acrylic, polycarbonate, and a type of carbon fiber panel. SDS extruders come in 4 different sizes, 5 ml, 10 ml, 30 ml, and 60 ml. Originally a 60 ml module was used with 60 ml syringes, however, due to the small amounts of ink being used, the 60 ml syringe contained too much air and upon extrusion would compress the air first before building up enough pressure to cause ink to extrude. This became problematic since the internal pressure could not be monitored or controlled, causing the ink to keep being deposited even after the stepper motor tried to retract. This resulted in loss of control of trace width and layer height which ultimately led to puddles of conductive ink that did not resemble any design. Only filling the 60 ml syringe up first appeared to be an adequate solution, but the steeper motor that actuates the ball screw bottoms out when there are very small amounts of material loaded into the

syringe. To combat this problem a 5 ml SDS head was purchased so that smaller amounts of ink could be used without creating too much waste due to unwanted pressure built up by compressed air that keeps expending ink even when the lead screw stops turning. The use of the 5 mL syringe deposition device solved all issues due to controlling flow of material from the syringe. After leveling the stage of the printer and running trial prints the appropriate nozzle velocities, flow rates, and z heights were optimized so that the traces that were laid on the substrate matched the desired paths that were designed using CAD software. When using the Bare Conductive paint, since this material is more viscous, a blunt tip needle with an inner diameter of 0.26mm was used. The stepper motor received 0.750 pulses per nano liter of fluid and the head moved at a speed of 1mm/s. When creating traces using the ink purchased through Chem^3 which had a very low viscosity, the inner diameter of the blunt tip needle used is 60μm, the head velocity was set to 3.5mm/s and the stepper motor received 0.750 pulses per nL. The values acquired for each printing process were gathered experimentally through a series of prints. Flow rates had to be set based on nozzle size and velocity had to be increased or decreased depending on how well the fluid would flow. The z layer height set for both inks was set to 100μm and was the only constant set based off the CAD designs to show that high resolution could be attained using the proposed system of fabrication. Having an enclosed printing environment with a heated printing surface allows for the whole build envelope to heated and minimize heat loss to the outside environment. This is helpful during the sintering process since the substrates that the traces are printed on are not always the best at conducting heat. The traces

created using Bare Conductive inks do not need to be sintered as they are conductive once the paint has been allowed to dry. When printing with Bare Conductive inks, the heated bed was left off due to the nature of the paint. Once these traces were laid and sintered, a clear protective layer was painted over them leaving just the ends exposed for the connection of lead wires either by soldering or the use of a conductive glue or paint like the one made by Bare Conductive that was used for creating traces in the screen printing section. Testing and characterization of the sensors created using these techniques can be found in the testing and results section.

CHAPTER 3

EXPERIMENTATION

To verify the accuracy and usefulness of each different sensor created and see which one works the best, each type of sensor underwent a specific set of tests and characterization processes. First, resistance was tested using benchtop digital multimeters. If the test equipment was able to verify a change in resistance or capacitance the sensor would be characterized by applying loads in an increasing manner to the sensor while output data in the form of resistance change or voltage output was collected using a benchtop digital multimeter. The data collected was then used to characterize the sensors created to analyze the accuracy of each sensor created using one of the many methods described above for fabrication processes.

3.1 Preliminary Tests

3.1.1. Aim

The objective of the test was to compare the force sensor created using conductive copper tape and Velostat to force sensors currently available on the market. The experiment tested the working range of the sensor and looked at hysteresis in the fabricated sensor when compared to hysteresis from commercially available sensors.

3.1.2. Testing Methods for Piezo Film Sensors

To test both the fabricated and commercial sensors, each sensor was placed on top of a force plate and zeroed out so that the resulting forces read were equal to zero. Weights of different sizes were then placed on top

of a round metal bar which acted as the first weight to ensure that the load was evenly distributed over the area of the actual sensor. Weights were applied one by one left for a few seconds so that the reading from the sensor could stabilize. After the reading had stabilized the reading from the sensor and the weight were recorded and entered into an excel spreadsheet. Once all the weights had been added and the final sensor reading was collected, the process began in the reverse order. Weights were removed one by one again allowing a few seconds in between for each weight so that it could be verified that the reading being shown would not fluctuate. Figure 25 shows the resulting force vs sensor reading as output by the Arduino and the strain gauge module assembly as seen in figure 22 above. To generate the second graph in figure 24 all tests were run in the exact same order as previously described with the only difference being that the sensor, instead of being hooked up to an Arduino strain gauge module combination, was hooked up so that actual resistance change would be recorded.

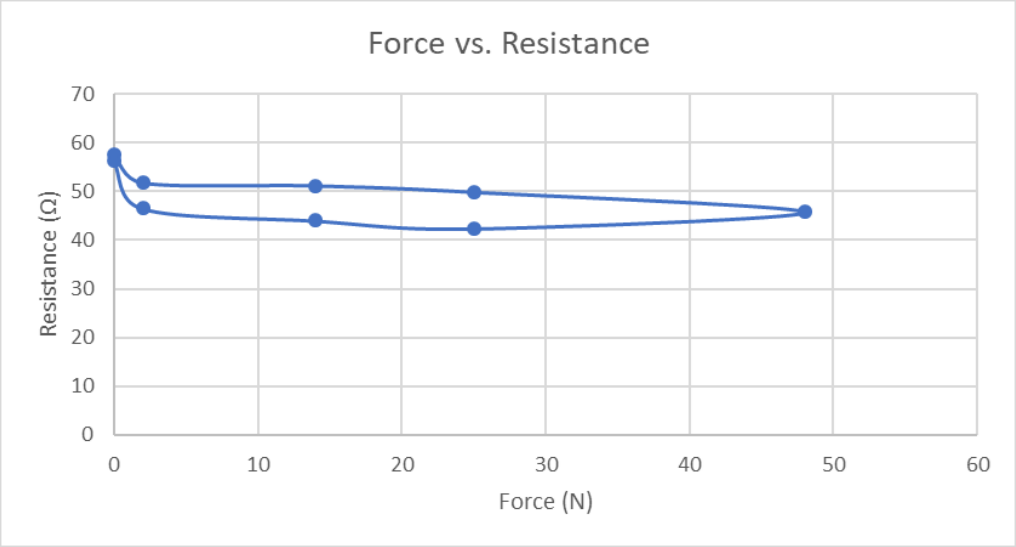

Figure 24: Characterization graph for sensor

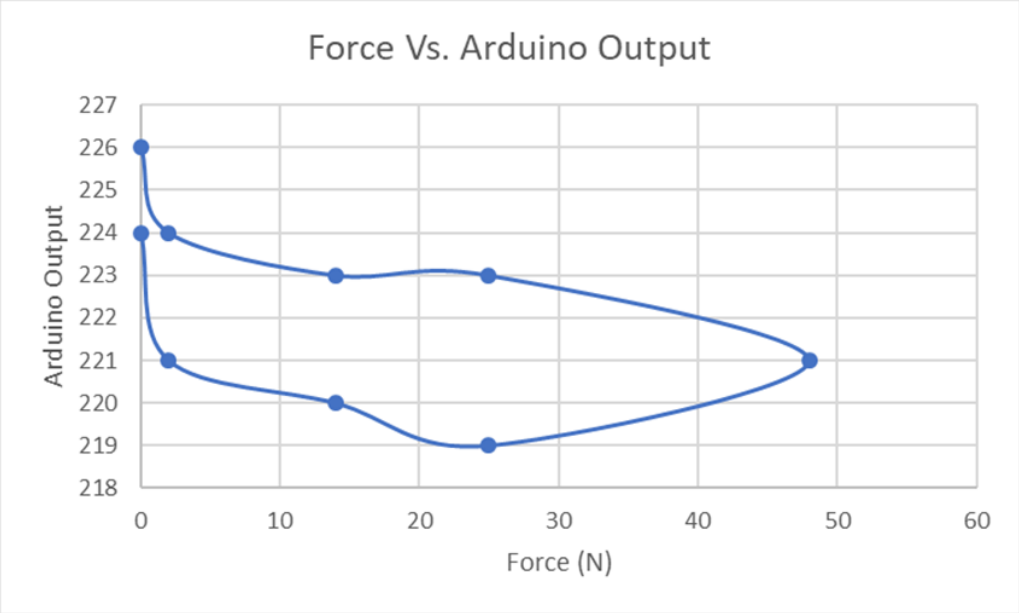

Figure 25: Characterization graph for sensor

3.1.3. Interdigitated Finger Sensor (FSR) Testing and Results

The interdigitated finger sensors, described in the FSR section above, were built and tested in a series of steps. Four sensors were created, pictured above, and tested. The results of the tests found that the closer the space and trace of a sensor are, the better response. Test results from the 3mm, 5mm and 7mm space and trace patterns can be found in the appendix and were not selected to continue development on for their lack of repeatability as well as becoming oversaturated when experiencing similar loads applied to the 1mm sized spaces and traces. Using the individual sensors design, 12 sensors designed exactly the same way using the same spacing and same sizing were cut using a vinyl cutter. The sensors were spaced and arranged to develop a 3x4 matrix mat that is able to sense different forces at different locations. A voltage divider circuit discussed in the design part of this paper was built and hooked up to each sensor as loads were applied to collect the sensors response. This was done multiple times on each of the 12 sensors in the mat. Unfortunately, due to some unforeseen issues, sensor 4 and 10 although somewhat responsive, failed to produce meaningful results. This will need to be looked at in the future and should be very easy to combat since all sensors were made using the exact same process. Failure of the sensors can be attributed to human error and are not indicative of the results obtained as will be proven in this section. Figure 26 shows testing conditions and the voltage divider circuit that was utilized can be seen. The voltage divider circuit was made using a 10kΩ resistor for R_1 and R_2's value comes from the resistance of the FSR before any load is

applied. The resistance value of the FSR's that was measured before any load was applied ranges from 8.3 kΩ to 27.8 kΩ. These values with no loads are outliers and even though they are greatly varied, do not have an effect on the accuracy of the sensors response when loaded. The voltage divider circuit can be seen in the appendix.

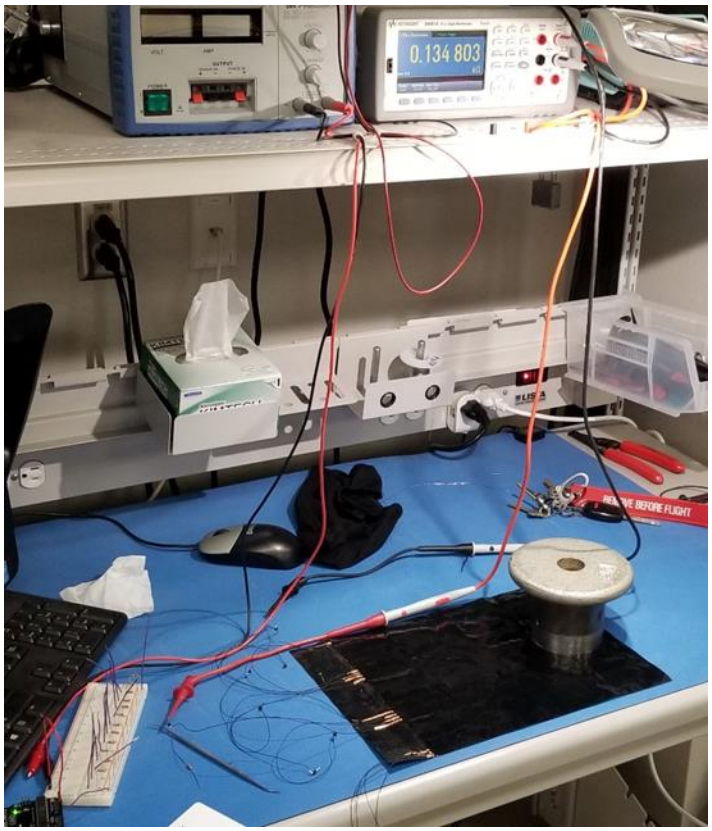

Figure 26: Testing of FSR mat

Looking at the literature describing FSR design and characterization, it is pointed out that the response of the sensors can be well approximated by some function of the general form:

$$y = ax^{-b}$$

When plotting the response, the sensors resistance is the dependable variable and the input variable is the load applied. As shown above, when not plotted on a logarithmic scale the data is nonlinear. However, this data reflects the same characteristics as the commercially available sensors. Figures 27 show a few responses gathered during testing.

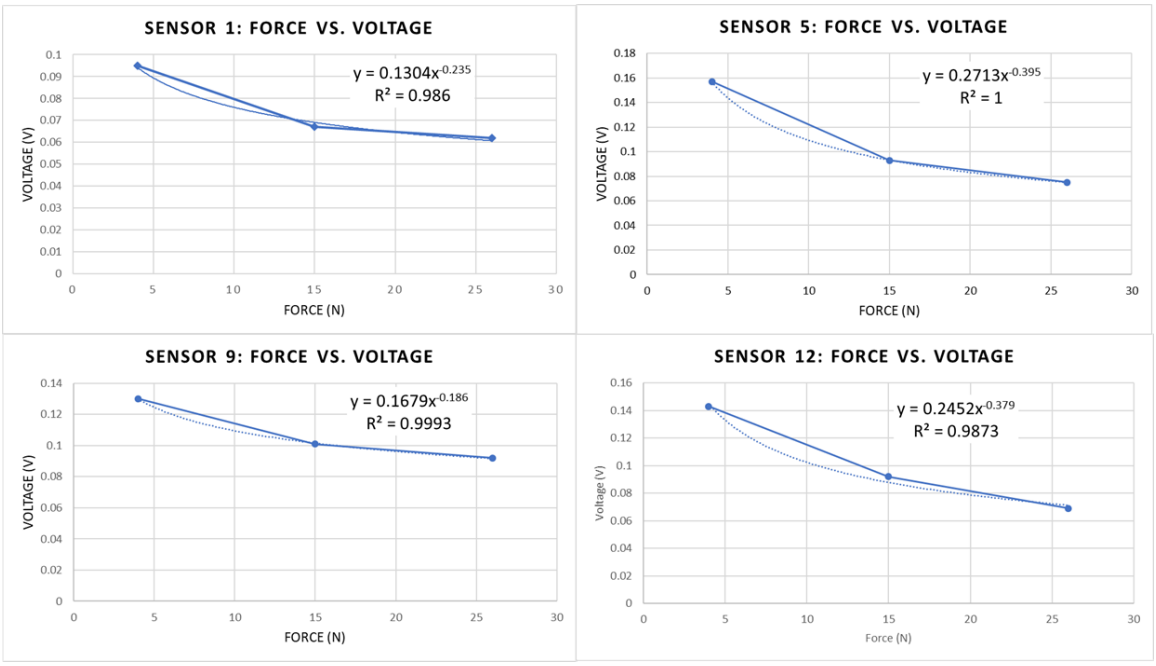

Figure 27: Force Vs Voltage responses for FSR sensors

A power equation was fit to the data collected during the loading of the sensors and are matched very accurately with results seen in commercial sensors mentioned above and follow the same type of characteristic equation that is expected of resistive type sensors. These responses are nonlinear as the literature suggests will happen. When plotting on a logarithmic scale for the x and y axes, once again as the literature suggests, the results become near linear if not completely linear. It is expected that curve data will vary widely according to sensor size, design,

and construction but the main focus is that the approximate shape of the curve and the equations obtained from such curves are in agreement with research done on FSR's and resistive type sensors. The logarithmic scaled graphs can be seen below in figure 28.

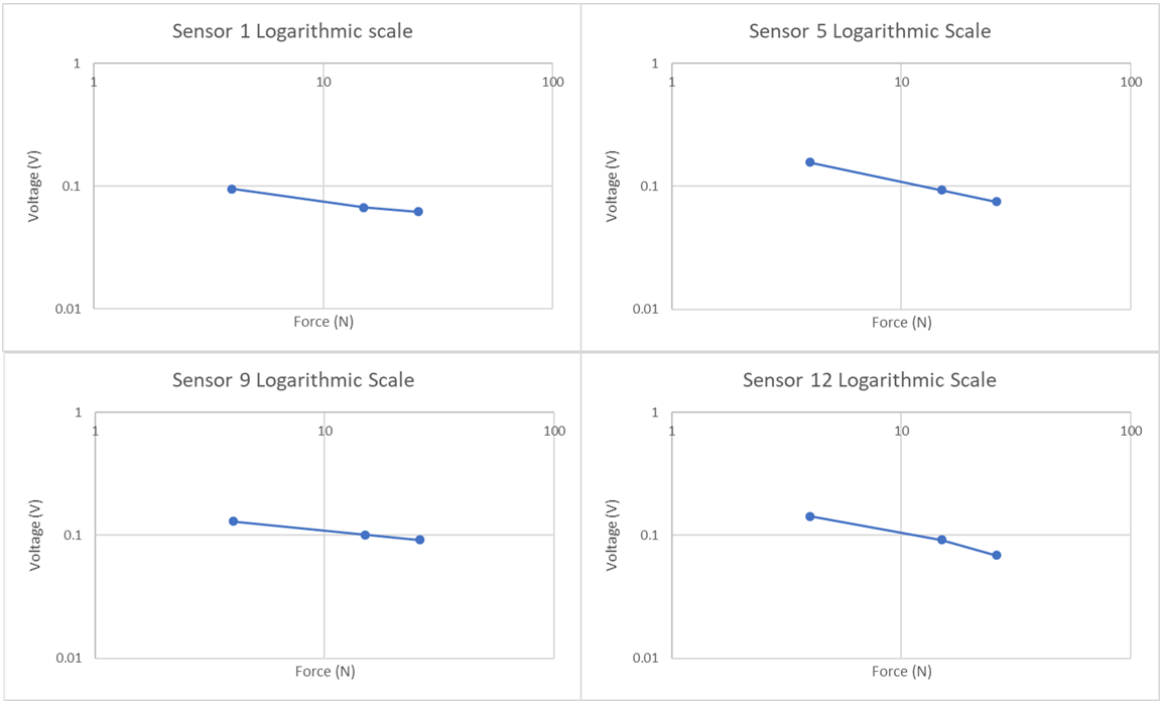

Figure 28: Force Vs Voltage responses plotted on a logarithmic scale

It is important to note that placement of the load, how the sensors are mounted or where they are placed, and how the sensors are actuated can all greatly affect the characteristic curves. For the data obtained during the testing part of this project careful consideration was taken to ensure that all experiments were repeated identically, and that all information was

collected using the same methods as to not affect the results to illicit a desired response.

Using Matlab, heat maps displayed in figures 29, 30, 31, and 32 were created from the data collected on the discrete array of sensors that show voltage intensity as loads are applied to the sensors in the array. The heat maps shown below show 4 different conditions, the first of which has no load applied. The second heat map was generated after a load of 4 N was applied. The final 2 heat maps show the voltage response after 15 N and 26 N were applied respectively.

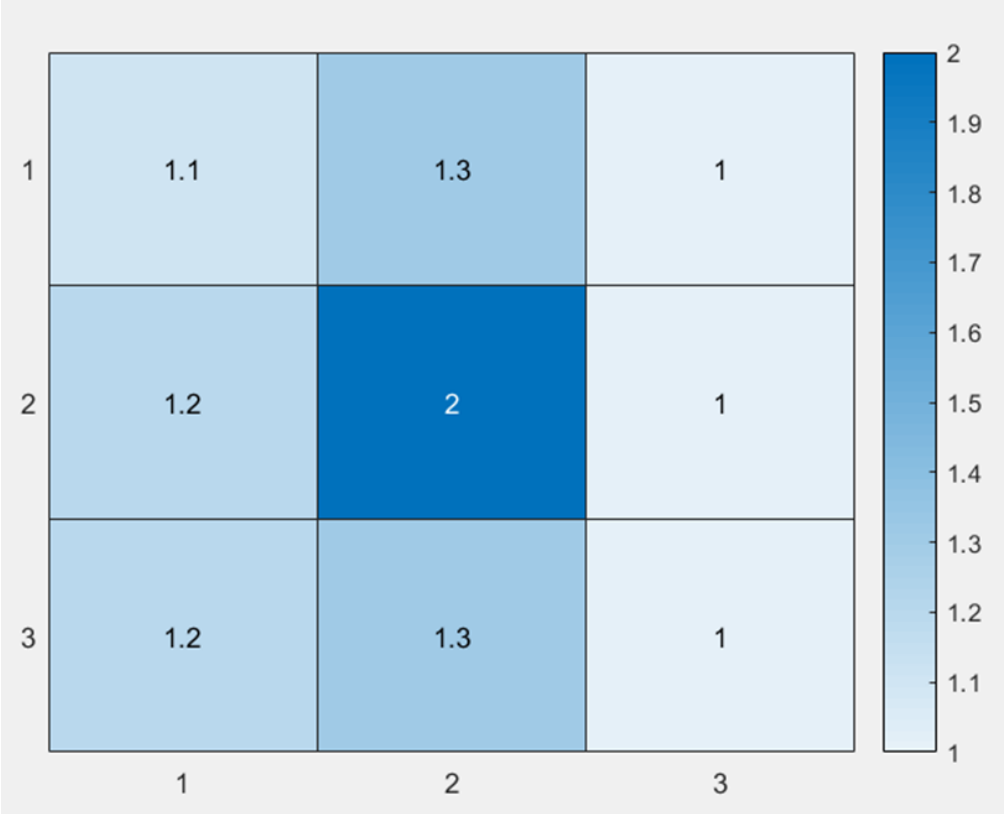

Figure 29: Heatmap of sensor mat with no load

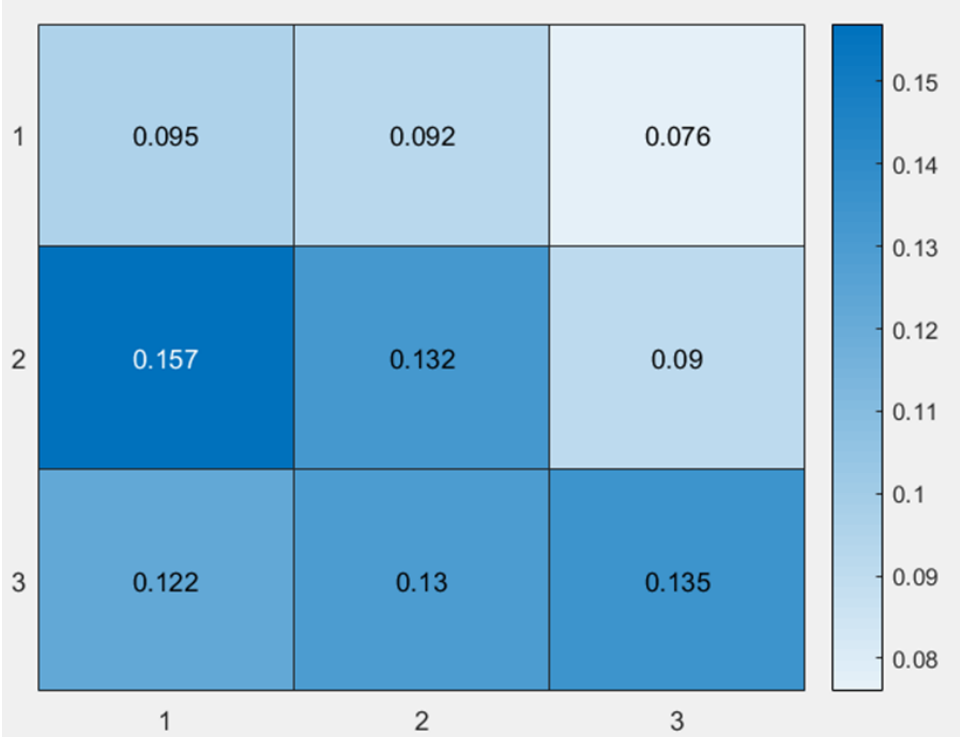

Figure 30: Heatmap of sensor mat with a 4N load

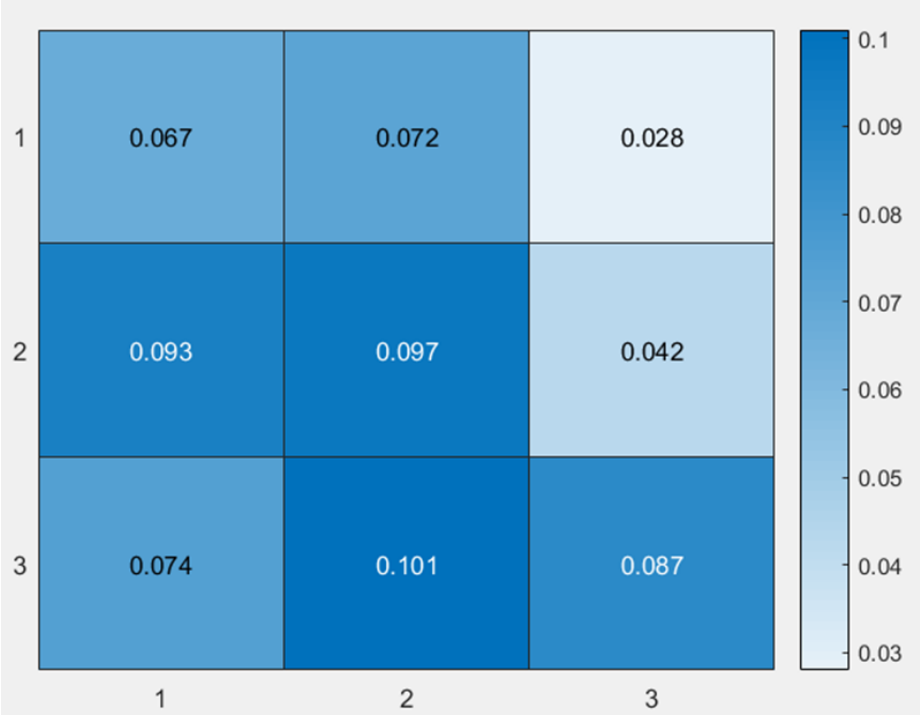

Figure 31: Heatmap of sensor mat with 15N load

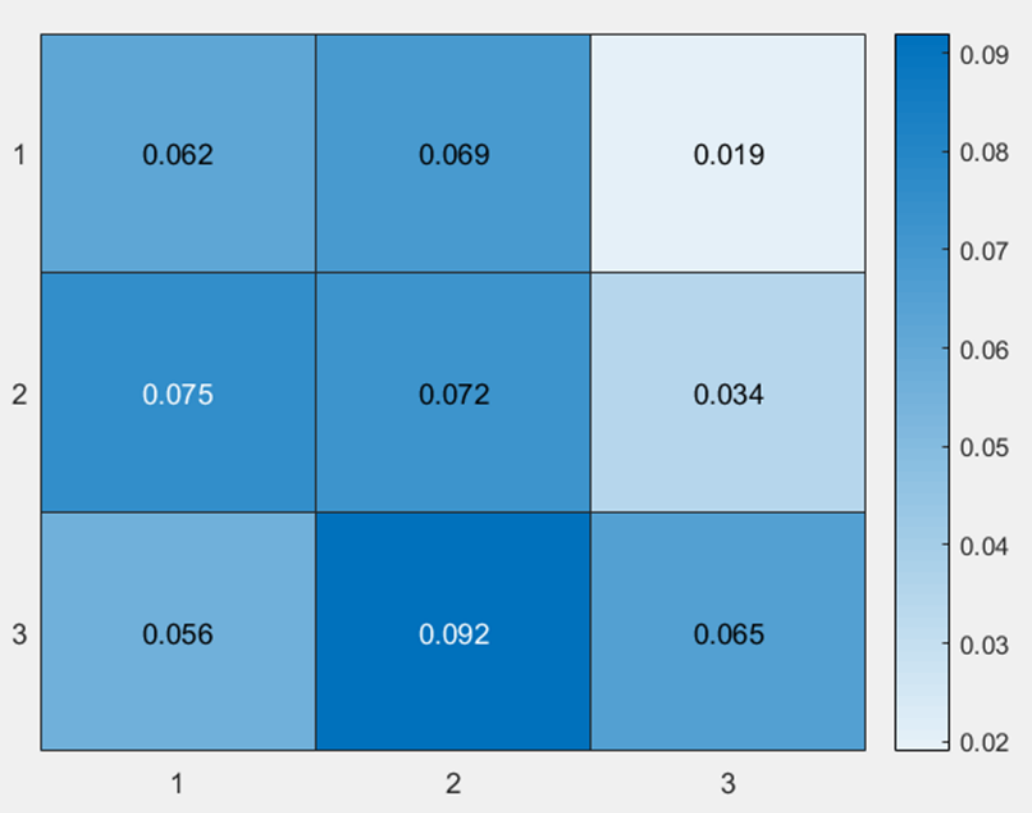

Figure 32: Heatmap of sensor mat with 26N load

3.1.4. Foil Strain Gauge Testing Results

To test the foil strain gauges, the backing was removed from the vinyl that the foil sensors were cut onto. By removing the backing and revealing the adhesive, the foil strain gauges could be placed directly onto the items they would be measuring changes in. This ability to create custom strain gauges that already have an adhesive attached is valuable because not only are the strain gauges cut to specific shapes and sizes which allows for fully customizable cheap strain gauges, but specimen preparation procedures are strain gauge adhesion times are shortened. The custom foil strain gauges were tested using a strain gauge module that is shown in figure 22. The strain gauges were soldered to the original leads coming from the strain

gauge module and were also attached using longer leads where applications called for the strain gauge to be placed further from the strain module.

The strain module was connected to a Arduino bluno which is a small microcontroller with Bluetooth capabilities. Once the module was installed and programmed, an app could be downloaded to a researcher's cell phone or laptop that directly connected with the Arduino Bluno module making the transfer of data quick and wireless while giving real time results. Pads were placed next to the leads so that resistors could be wired up to the actual custom strain gauge allowing the user to offset the resistance to a desired value before placing it on the object that would be monitored for change. Another excellent capability of these custom foil strain gauges is that with the combination of additive manufacturing, the strain gauges can be inserted into the actual part that is being printed. The way this was demonstrated was by pausing a print of a dog bone structure just long enough to place the sensor in the middle of the object. Once the sensor was positioned the print was resumed and since the thickness of the sensor is negligible compared to the height of the layer being deposited, there was no effect in overall print quality showing that this specific application can be repeated using a myriad of thin sensors on a number of different structures that are created using additive manufacturing.

The foil strain gauges behaved in the same manner as the conventional strain gauges that came attached to the strain modules. When these original strain gauges were replaced the only difference seen was the initial values

which are dependent on the resistance of the actual sensors themselves. When either the commercial or custom made strain gauges were in use they exhibited the typical properties you would expect to see in the response from strain gauges. When the sensors were put into tension the resistance increased and alternatively when put in compression the signals showed that the value of resistance decreased. The use of an onboard potentiometer allows for setting a zero point before starting testing. This part of the setup would require a little bit of extra time, not much however, and would need to be done for each different application of different strain gauges created. By adjusting these zero points or adding in resistors, these wireless transmitting modules and custom strain gauges could be beneficial in multiple different areas where custom, cheap, flexible sensors are concerned. The wireless transmission capabilities also open many useful applications including putting strain gauges in areas that are too small to accommodate a DAQ to collect the data being transmitted and are also very useful for applications where strain gauges need to be added and removed constantly so conditions can be monitored, such as on airplane components.

3.1.5. Screen Printing Results

The screen-printed sensors didn't give desired results. When creating the masks to fabricate these sensors, the fine spacing and small structures that needed to stay in place to result in successful screen-printed strain gauges often did not stay put resulting in strain gauges with non-uniform trace width and sensors that weren't repeatable when trying to replicate. This is believed to be attributed to the materials used for making the screen printing

masks and the methods used to make the masks. While traditional screen printing materials could have been acquired, the focus of this paper is to create custom, cheaper than commercially available sensors. This can still be achieved using screen printing inks and fabrication methods but will need to be delved deeper into in future works. Failure to come up with a repeatable process that yields similar working strain gauges can be attributed to using inks not common in screen printing as well as the creation of masks that were not rigid enough to hold their patterns for the whole screen printing process.

The results, some of which can be seen in figure 23, resulted in sensors that could not be used. The process to apply these strain gauges becomes more difficult than conventional methods making this particular way of utilizing screen printing for sensors unattractive for the foreseeable future. Future work will aim to utilize better inks and ingenuity for coming up with a process for making custom masks that work far better than what was found using thin semirigid plastics and paper products. Different process on different materials in the future have the potential to give consistent repeatable results which were not fully realized while trying to come up with an unconventional screen printing method of manufacturing and applying strain gauges.

3.1.6. Planar printing/direct writing sensor testing

Sensors created using planar writing techniques were created using a Hyrel System 30M as described above in chapter 2 section 2.5. To test the sensors,

multiple strain gauges were printed on different shaped substrates of different thicknesses, either 1/4’ or 1/8’ acrylic. The BareConductive ink gave the best results when creating the sensors because the Chem^{3} ink has a low surface tension which caused the very thin traces, that came from a blunt tip needle with an inner diameter of 60μm, to spread and bleed into each other. BareConductive sensors were printed on 1/8th inch thick acyllic substrates some of which were cut into dog bone shapes using a laser cutter. These samples can be seen in figure 33 and figure 34 respectively.

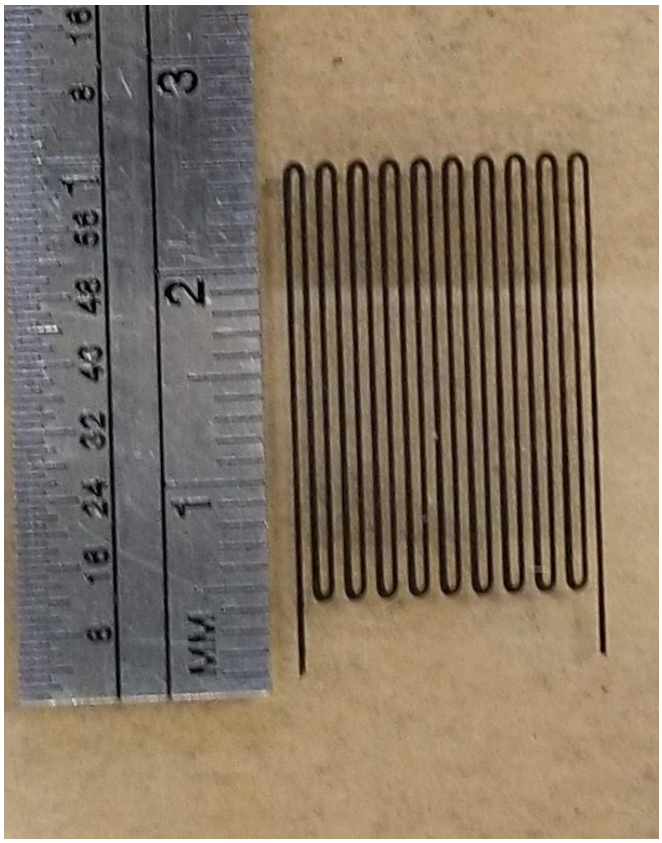

Figure 33: Strain gauges printed on acrylic using Bare Conductive Ink

Figure 34: Strain gauges printed on scrylic dog bones

The acrylic substrates not in dog bone configurations, were tested as cantilever beams. The strain gauge which was printed in the middle of the substrate was placed so that the center of the sensor would see the most bending when forces were applied. The back of the substrate was clamped to the work bench and a hole was drilled into the very end of the substrate so that weights could be attached in an increasing manner. Weights were attached one at a time and then the voltage output through the wheatstone bridge was recorded. These setups and testing methods can be seen in figure 35.

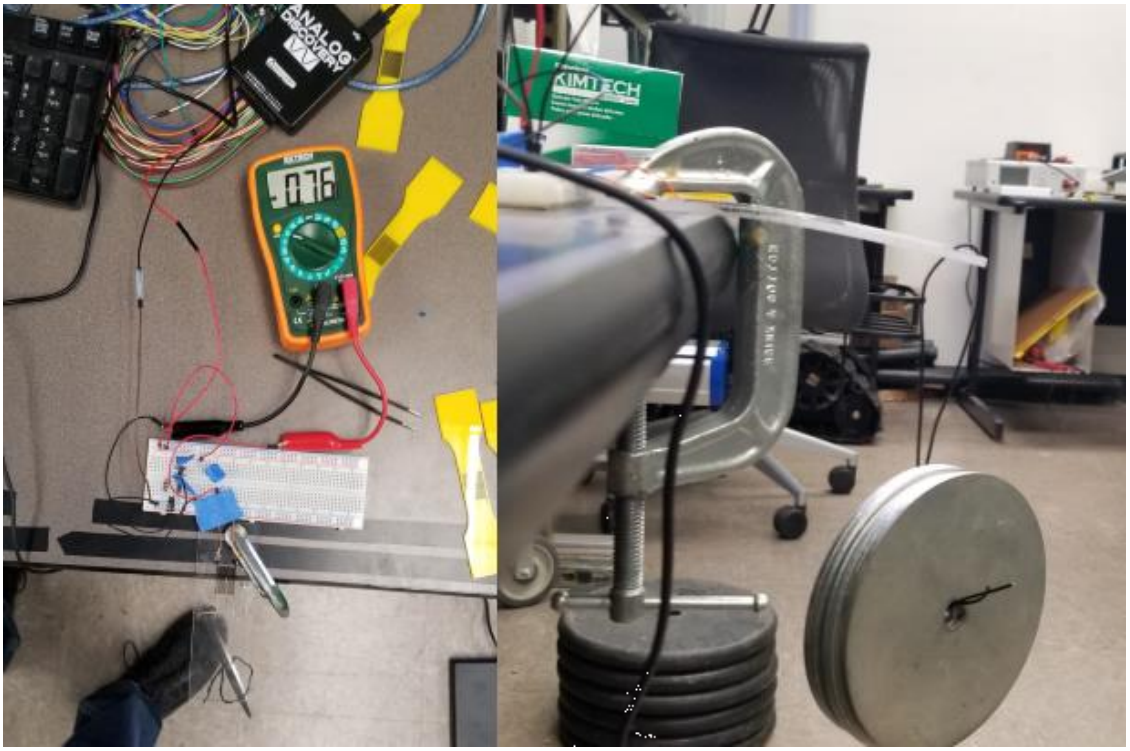

Figure 35: Test setup and testing pictures of Bare Conductive strain gauge

Each weight was placed on a thin wire with a hook at the end which allowed weights to be easily added and removed without causing too much disturbance to the sensor other than the loading and unloading of forces. A wheatstone bridge circuit was created using the sensors resistor value as R_x in the wheatstone bridge configuration, this was used to change the sensors passive resistance change into a transducer with an active voltage signal that could be read. The sensors resistance varying when loads are applied is what causes the voltage to increase or decrease. In the case of the cantilever beam with the sensor placed on top, due to the wheatstone bridge configuration and the resistor values used the voltage dropped as more load was applied. Loads of 2 newtons were added incrementally and the load and output voltage were recorded. The wheatstone bridge resistor values and circuit

configuration can be found in the appendix. Both sensor responses, when fitted with a linear trendline, showed a very linear relationship to applied load and voltage output. The graphs shown below in figure 36 and 37 show the values collected during testing and the relationship between the loading and voltage outputs.

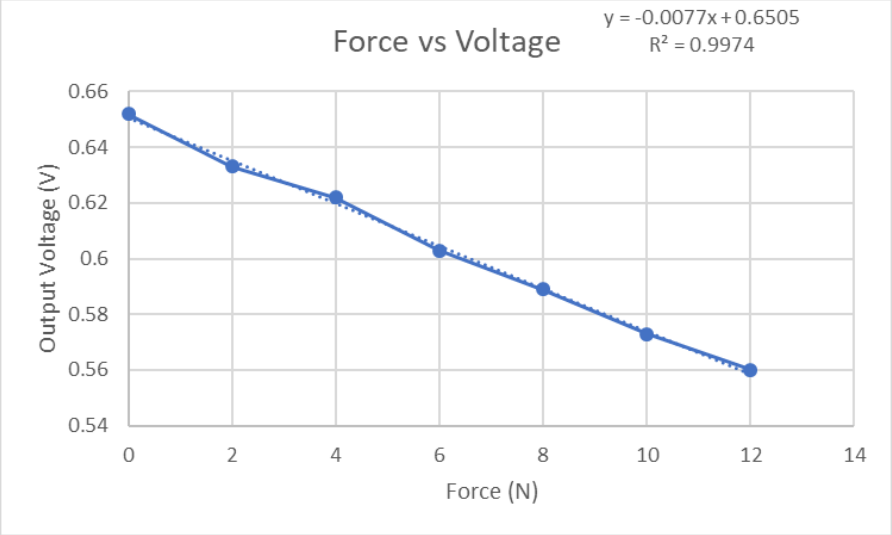

Figure 36: Force vs Voltage output for cantilever testing of Bare Conductive sensor

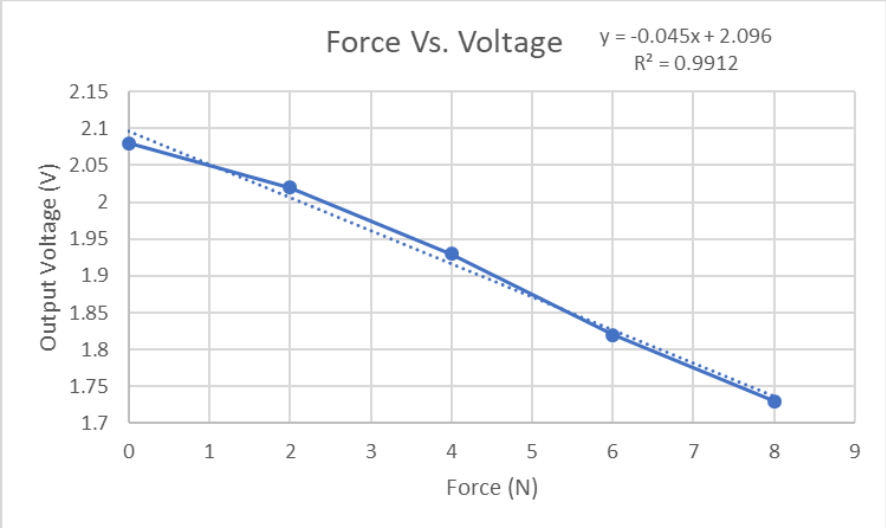

Figure 37: Force vs Voltage output for cantilever testing of another Bare Conductive sensor

Chem^3 sensors were tested in a similar manner but were tested for dynamic response instead of just loading. Panels with sensors printed on them created by Chem^3 were fixed to a workbench and bent down until significant bending was experienced. The load was removed instantly and the board containing the sensors was allowed to vibrate freely until the response showed no change. The test setup is shown in figure 38. The graphs in figures 39 and 40 show the frequency response of the sensors as the board vibrated and then came to rest. These frequency tests were performed to show how these types of printed sensors would behave when experiencing vibrations that may be seen if these sensors are attached to an aircraft. Four point bending and three point bending tests were also conducted in the SIM building at the ASU polytechnic campus. The bending fixtures were loaded into an Instron testing machine and loads were applied and held to show the response of the printed sensors under non-dynamic conditions. The results from this testing and the test setup are shown in figures 41 and 42.

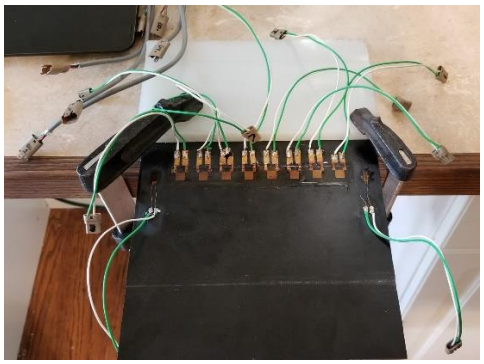

Figure 38: Chem Cubed sensors dynamic testing setup, commercially available Omega strain gauges attached for reference

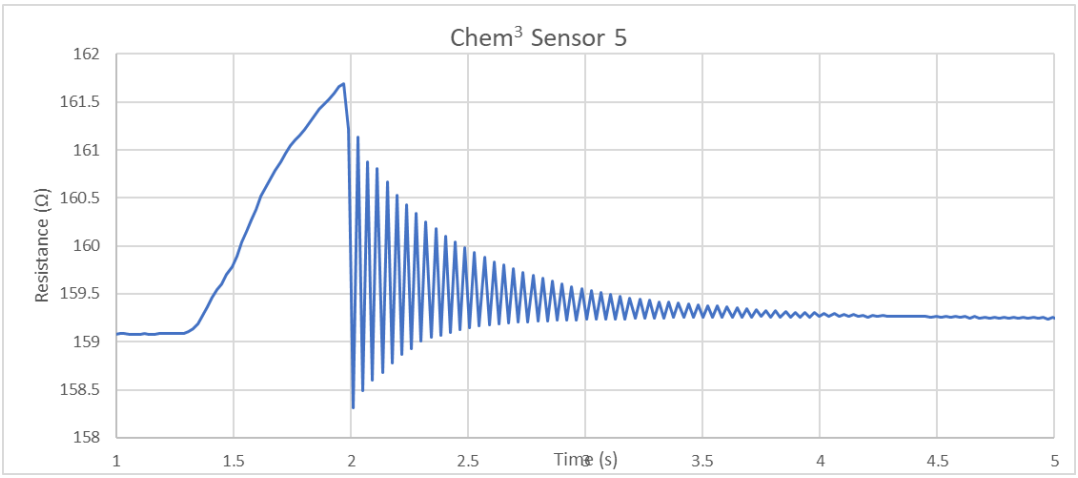

Figure 39: Frequency response of Chem Cubed sensors

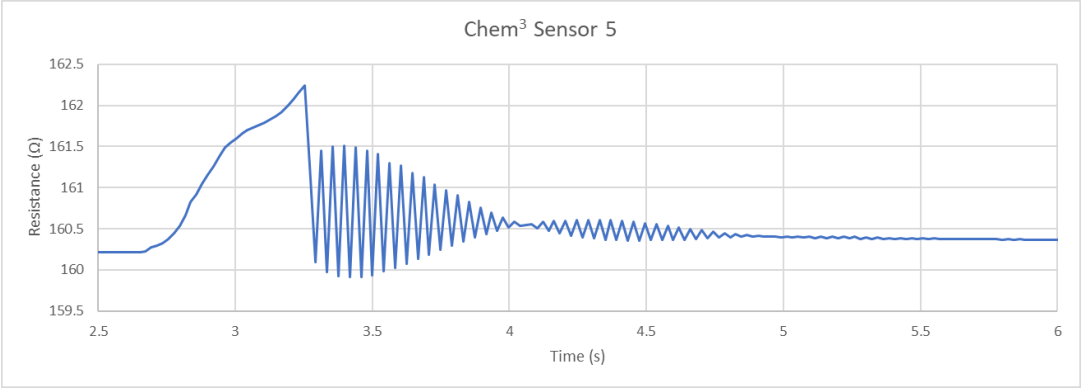

Figure 40: Frequency respone from Chem Cubed different dynamic test

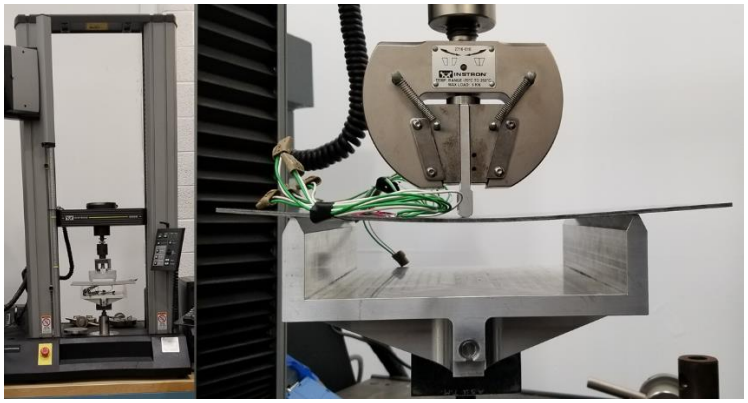

Figure 41: 3 and 4 point bending testing

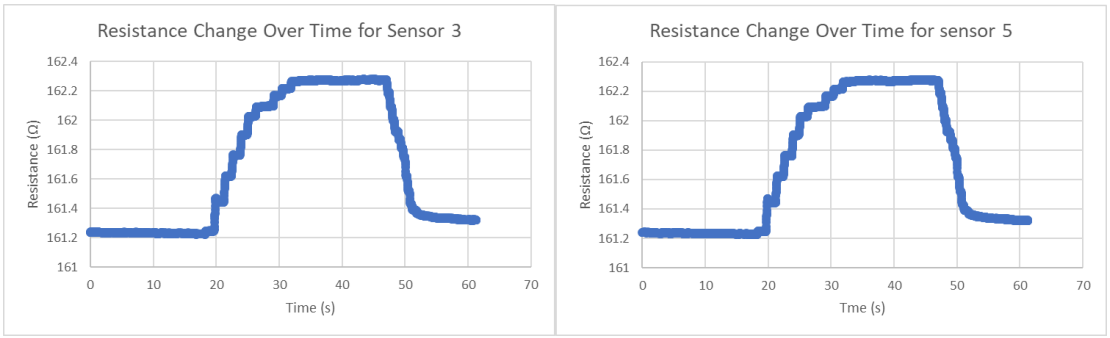

Figure 42: Resistance responses to loads applied during 3 and 4-point bending tests

Sensors printed on the dog bone shaped pieces of acrylic were loaded into a tensile testing machine and were gradually loaded. A load cell placed on the bottom of the frame where the hydraulic piston comes into contact so that smaller loads could be measured since the load measuring apparatus affixed to the machines smallest readable load size is .5 kN. The sensors started with no load and loads were gradually applied until the sensor exhibited a change in voltage. The testing setup can be seen in figure 43.

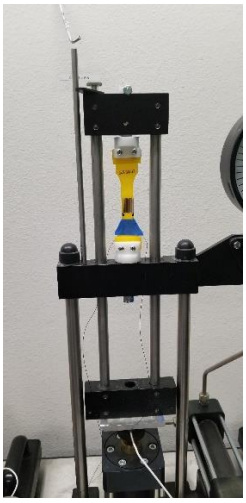

Figure 43: Tensile testing of sensors printed on dog bones made from acrylic

Once the voltage output showed any change, the load was left, and the sensor output and load input were recorded. After the information was recorded, the load would be increased until further changes in output voltage could be seen and recorded. Due to how the dog bones were secured in the tensile testing apparatus, sometimes the dog bones would crack or break. The data that was collected from these tests still show the sensors response to strain and did not have any ill effects on the information that was collected. Once the experiments were complete and the data was recorded, linear trendlines were fit to the data showing R^2 values ranging from 0.96-0.99 indicating a good fit of the data to a linear response. The data, trendlines, and equations for the trendlines can all be seen in figure 44.

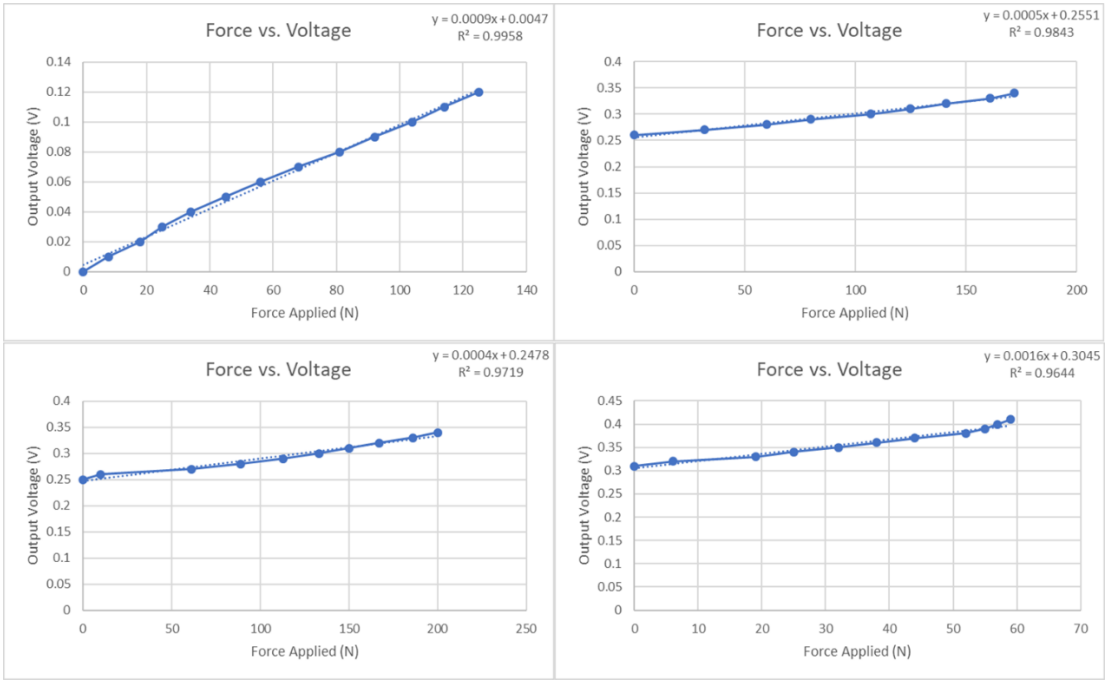

Figure 44: Near linear resonses from tesnile dog bone testing of prnted sensors

CHAPTER 4

CONCLUSIONS

This extensive work on flexible sensors using non-conventional methods provides results showing that sensors can be custom made using materials and methods not used in conventional processes. The sensors created cost less than commercially available sensors and strain gauges and fabrication processes were simple when compared to the complex methods that are currently used to create commercial sensors and strain gauges. The foil strain gauges were able to be used when hooked up to a Bluetooth Arduino Bluno and a strain module and gave results of the same caliber that the strain gauges attached to the strain modules produced. The results were also able to be wirelessly transmitted to a mobile phone or laptop for real time, wireless sensor data transmission. As stated in above sections these implications are great for applications of placing strain gauges or other sensors in hard to reach areas that do not allow space for a data acquisition system.

The FSR's that were made from conductive copper foil with conductive adhesives, gave results identical to the results that Sensitronics, a company that makes commercially available sensors, shows on their website. When fitting a trendline to the data collected the power series trendline was of the form:

$$y = ax^{-b}$$

Showing that FSR's can be made with much cheaper materials while still yielding the same results. This is promising for applications where researchers would be able to create their own custom sensors for novel applications without much lead time.

The strain gauges printed on acrylic substrates give promising results for sensors created using conductive inks. During both bending tests and tension tests, the data collected showed that the output behavior of the strain gauges was linear. To make the output linear a Wheatstone bridge circuit must be utilized. These strain gauges printed with Bare Conductive ink are also a promising solution to creating custom size and application strain gauges on multiple types of surfaces. The strain gauges do still require surface preparation to ensure that the ink will adhere to the substrate that it is being printed on and they require the use of a sealing agent to ensure that the sensor is not damaged.

The results from this thesis show how possible it is to create accurate sensors that cost less than what is commercially available. With the myriad of sensors that are currently commercially mass produced, there is no end to the types of sensors that could be created and made functional using other non-conventional methods. By refining processes and experimenting with many more materials, the possibilities for types of sensors that can be created and implemented into personalized health-monitoring, human motion detection, human-machine interfaces, and soft robotics are endless.

References

Amjadi, Morteza et al. “Stretchable, Skin-Mountable, and Wearable Strain Sensors and Their Potential Applications: A Review.” *Advanced Functional Materials* 26.11 (2016): 1678–1698. Web.

Bao, Zhenan et al. “High-Performance Plastic Transistors Fabricated by Printing Techniques.” *Chemistry of Materials* 9.6 (1997): 1299–1301. Web.

Bentley, Derek, Lord Bingham, and Lord Goddard. “Introduction 1.1.” *History* (1952): 1–12. Web.

Castano, Lina M., and Alison B. Flatau. “Smart Fabric Sensors and E-Textile Technologies: A Review.” *Smart Materials and Structures* 23.5 (2014): n. pag. Web.

Ciminello, Monica, Rolf Evenblij, and Gianluca Amendola. “Sensor Systems for Smart Architectures.” *Morphing Wing Technologies: Large Commercial Aircraft and Civil Helicopters* (2017): 321–350. Web.

Gilleo, By Ken, and Et-trends Llc. “The First 105 Years of Flexible Circuitry.” 7. Print.

Giovanelli, Davide, and Elisabetta Farella. “Force Sensing Resistor and Evaluation of Technology for Wearable Body Pressure Sensing.” *Journal of Sensors* 2016 (2016): n. pag. Web.

Izdebska, Joanna. *Flexographic Printing*. Elsevier Inc., 2015. Web.

Joyce, David, and Michael Scott. “Force and Mass Determination.” *Strain* (2018): 107–122. Web.

Khan, Saleem, Leandro Lorenzelli, and Ravinder S. Dahiya. “Technologies for Printing Sensors and Electronics over Large Flexible Substrates: A Review.” *IEEE Sensors Journal* 15.6 (2015): 3164–3185. Web.

Lowry, Robert K. “International Symposium on Advanced Packaging Materials.” (1999): 94–99. Print.

Mech, Archives Civil. “Functional Fillers Electrical and Magnetic Properties.” (2017): n. pag. Print.

Muth, Joseph T. et al. “Embedded 3D Printing of Strain Sensors within Highly Stretchable Elastomers.” *Advanced Materials* 26.36 (2014): 6307–6312. Web.

Pan, George, and Michael Goryll. “No Title.” December (2014): n. pag. Print.

Sirringhaus, H et al. “High-Resolution Inkjet Printing of All- Transistor Circuits.” *Science* 290.2000 (2000): 2123–2126. Web.

Suikkola, Jari et al. “Screen-Printing Fabrication and Characterization of Stretchable Electronics.” *Scientific Reports* 6. December 2015 (2016): 1–8. Web.

Sun, Jie et al. “Extrusion-Based Food Printing for Digitalized Food Design and Nutrition Control.” *Journal of Food Engineering* 220 (2018): 1–11. Web.

There, S. “Materials and Fabrication Techniques 2.1.” (2018): n. pag. Print.

Voxel8. “Silver Conductive Ink Technical Data Sheet.” April (2016): 2143. Web.

Xu, Yuanyuan et al. *The Boom in 3D-Printed Sensor Technology*. Vol. 17. N.p., 2017. Web.

“06-Piezoresistor.”: n. pag. Print.

“All-Polymer Field-Effect Transistor Realized by Printing Techniques Author (S): Francis Garnier , Ryad Hajlaoui , Abderrahim Yassar and Pratima Srivastava Published by : American Association for the Advancement of Science Stable URL : Http://www.jstor.o.” 265.5179 (2018): 1684–1686. Print.

APPENDIX

Results from FSR sensors made with fingers and sacings of 3mm, 5mm, and 7mm.

3mm	
Force (N)	Resistance (Ω)
0	1190
22	1090
32	1010
43	980
66	940
181	870
66	770
43	840
32	860
22	900
0	1160

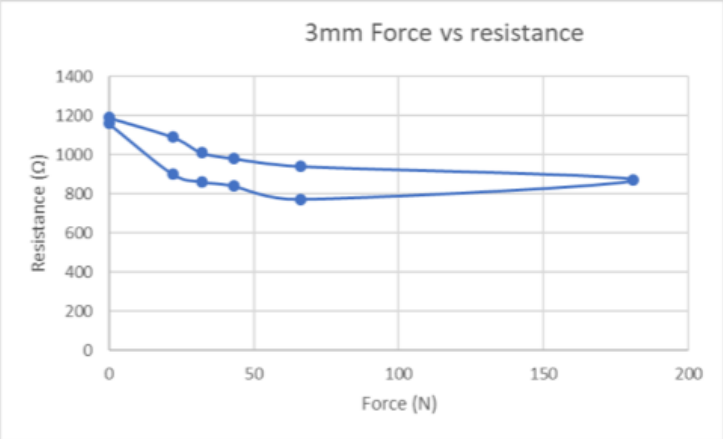

5mm	
Force (N)	Resistance (Ω)
0	1160
22	1080
32	980
43	930
66	810
181	780
66	730
43	780
32	830
22	900
0	1140

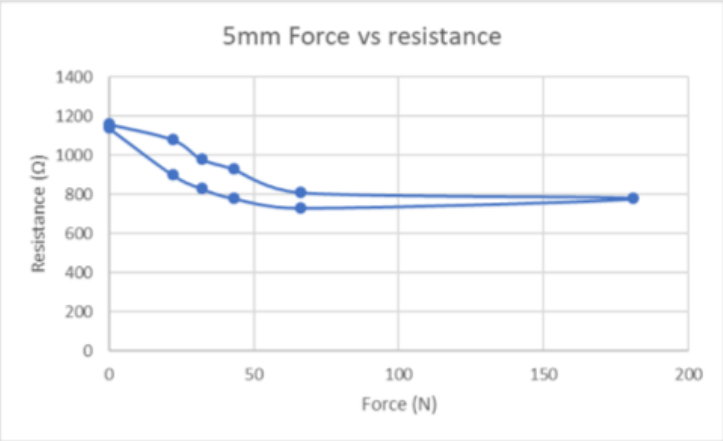

7mm	
Force (N)	Resistance (Ω)
0	3560
22	3270
32	2630
43	2440
66	2290
181	2360
66	2220
43	2360
32	2240
22	2310
0	2970

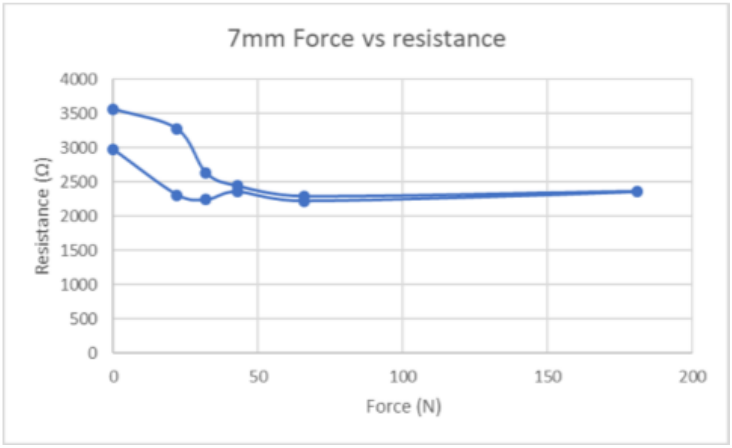

Wheatstone bridge circuits used for tensile testing of strain gauges printed on acrylic dog bones.

89.6 kΩ strain gauge

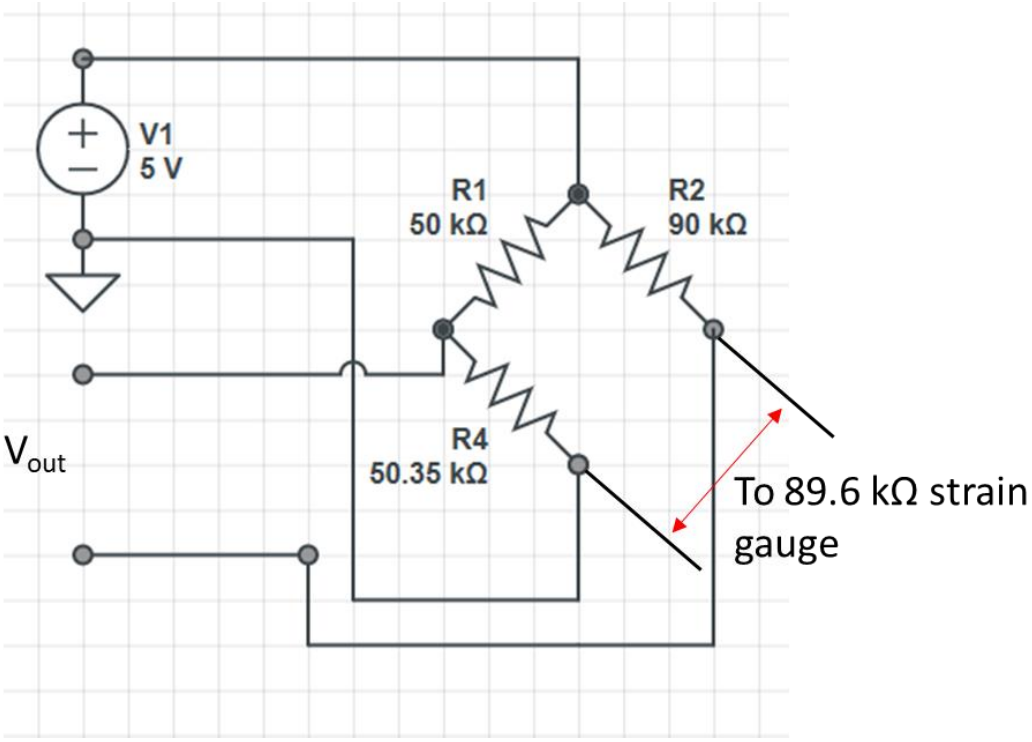

52.6 kΩ strain gauge

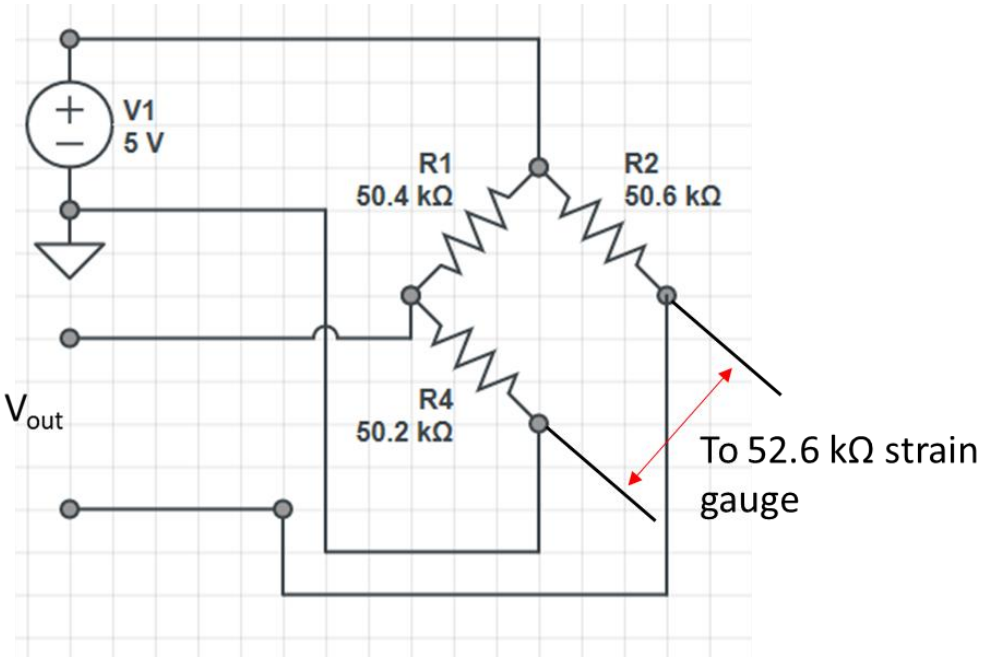

65.2 kΩ strain gauge

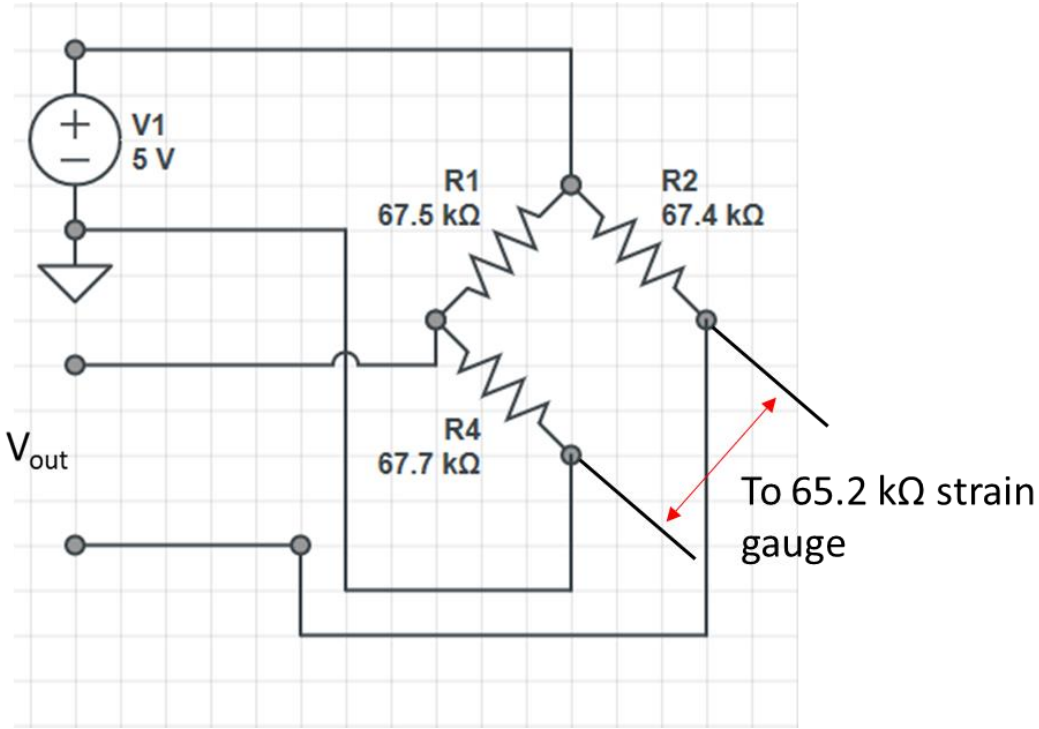

87.9 kΩ strain gauge

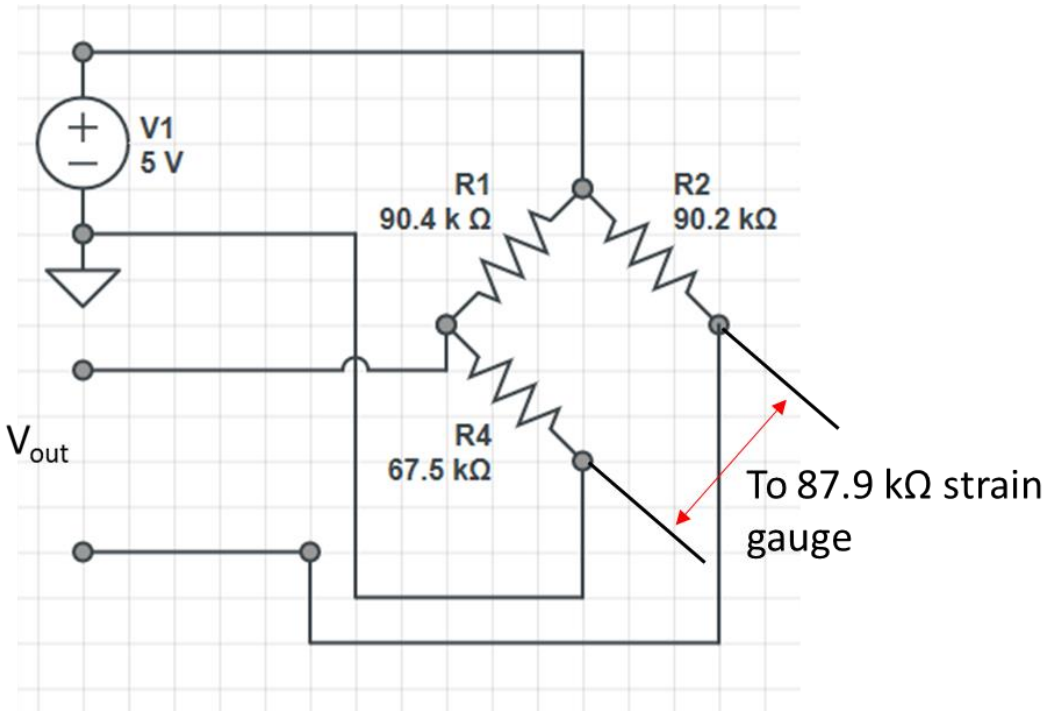

95.4 kΩ strain gauge

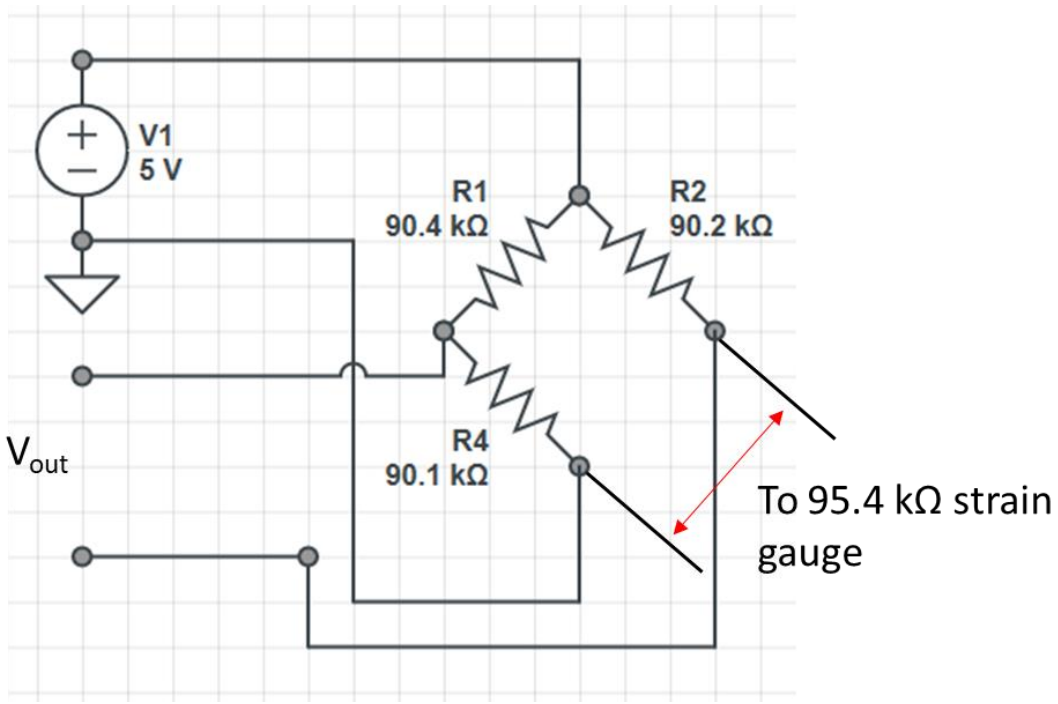

112.2 kΩ strain gauge

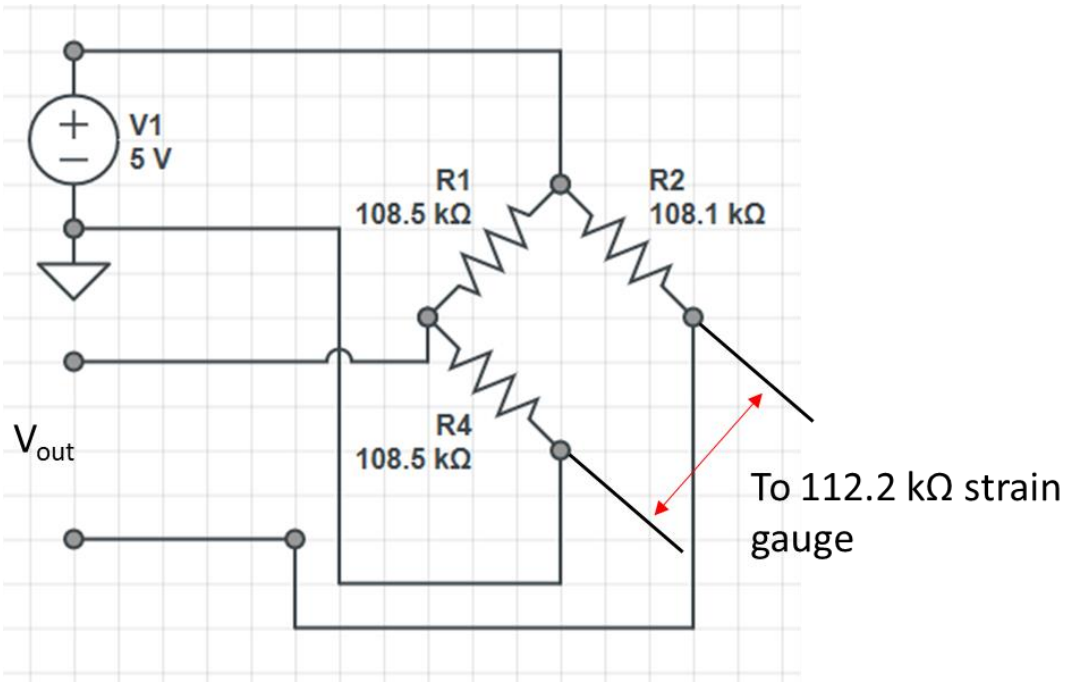

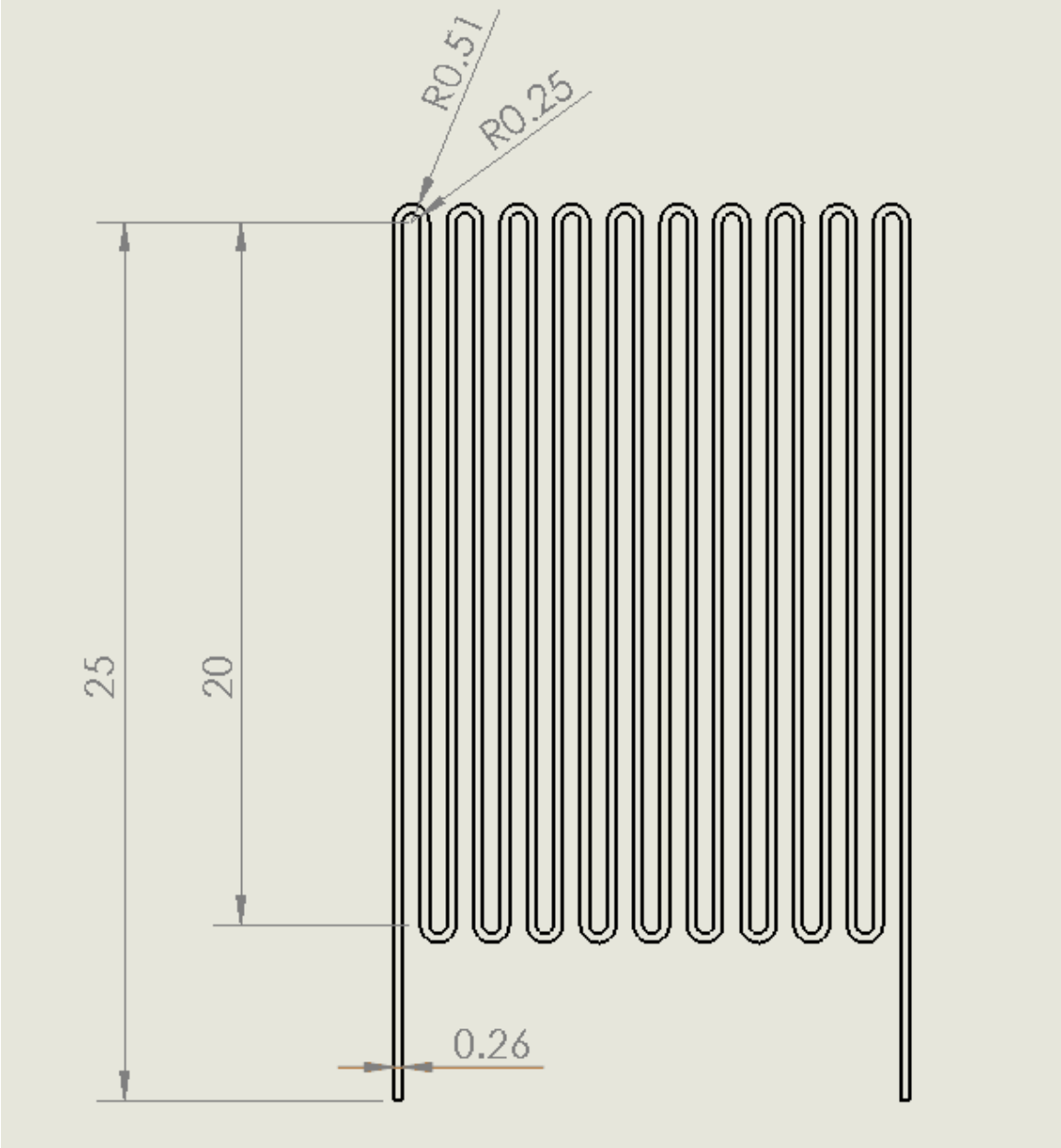

Measurements in mm

G-code for different printed strain gauges using Bare Conductive ink

; generated by Slic3r 1.2.9 on 2018-03-29 at 16:01:34

; external perimeters extrusion width = 0.26mm

; perimeters extrusion width = 0.26mm

; infill extrusion width = 0.26mm

```
; solid infill extrusion width = 0.26mm
; top infill extrusion width = 0.26mm

M107 ; disable fan
M104 T10  S0
G21     ; use millimeters
G90     ; absolute coordinates
G0 Z5 ; lift head to avoid collisions
G28 X0 Y0 ; home X and Y
G92 X0 Y0 ; reset origin: X and Y
G0 X0 Y0   ; move to desired origin
G92 X0 Y0 ; reset origin: X and Y
M83         ; relative extruder coordinates
;M109 S0  ;wait for temperture to come up.
M756 S0.1  ;set flowfor the first layer please


G21 ; set units to millimeters
G90 ; use absolute coordinates
M82 ; use absolute distances for extrusion
G92 E0 ; reset extrusion distance
;announce new layer <0>
;---
M756 S0.1
M790 ;execute any new layer actions
;---
G1 Z0.100 F1200.000 ; move to next layer (0)
G1 X147.220 Y90.246 F1200.000 ; move to first perimeter point
G1 X147.220 Y115.235 E0.00263 F90.000 ; perimeter
```

G1 X147.196 Y115.368 E0.00264 ; perimeter

G1 X147.138 Y115.478 E0.00265 ; perimeter

G1 X146.997 Y115.591 E0.00267 ; perimeter

G1 X146.871 Y115.624 E0.00269 ; perimeter

G1 X146.745 Y115.613 E0.00270 ; perimeter

G1 X146.581 Y115.521 E0.00272 ; perimeter

G1 X146.481 Y115.369 E0.00274 ; perimeter

G1 X146.460 Y115.235 E0.00275 ; perimeter

G1 X146.460 Y95.257 E0.00485 ; perimeter

G1 X146.437 Y95.117 E0.00487 ; perimeter

G1 X146.364 Y94.998 E0.00488 ; perimeter

G1 X146.258 Y94.915 E0.00490 ; perimeter

G1 X146.110 Y94.868 E0.00491 ; perimeter

G1 X145.957 Y94.890 E0.00493 ; perimeter

G1 X145.822 Y94.968 E0.00494 ; perimeter

G1 X145.735 Y95.095 E0.00496 ; perimeter

G1 X145.700 Y95.257 E0.00498 ; perimeter

G1 X145.700 Y115.235 E0.00708 ; perimeter

G1 X145.676 Y115.368 E0.00709 ; perimeter

G1 X145.640 Y115.443 E0.00710 ; perimeter

G1 X145.559 Y115.536 E0.00711 ; perimeter

G1 X145.477 Y115.591 E0.00712 ; perimeter

G1 X145.351 Y115.624 E0.00714 ; perimeter

G1 X145.227 Y115.613 E0.00715 ; perimeter

G1 X145.113 Y115.563 E0.00716 ; perimeter

G1 X145.021 Y115.479 E0.00718 ; perimeter

G1 X144.961 Y115.369 E0.00719 ; perimeter

G1 X144.940 Y115.235 E0.00720 ; perimeter

G1 X144.940 Y95.257 E0.00930 ; perimeter

G1 X144.919 Y95.123 E0.00932 ; perimeter

G1 X144.859 Y95.013 E0.00933 ; perimeter

G1 X144.763 Y94.925 E0.00935 ; perimeter

G1 X144.591 Y94.868 E0.00936 ; perimeter

G1 X144.465 Y94.879 E0.00938 ; perimeter

G1 X144.303 Y94.967 E0.00940 ; perimeter

G1 X144.215 Y95.095 E0.00941 ; perimeter

G1 X144.180 Y95.257 E0.00943 ; perimeter

G1 X144.180 Y115.235 E0.01153 ; perimeter

G1 X144.136 Y115.422 E0.01155 ; perimeter

G1 X144.057 Y115.525 E0.01156 ; perimeter

G1 X143.952 Y115.593 E0.01158 ; perimeter

G1 X143.831 Y115.624 E0.01159 ; perimeter

G1 X143.707 Y115.613 E0.01160 ; perimeter

G1 X143.593 Y115.563 E0.01162 ; perimeter

G1 X143.501 Y115.479 E0.01163 ; perimeter

G1 X143.441 Y115.369 E0.01164 ; perimeter

G1 X143.420 Y115.235 E0.01166 ; perimeter

G1 X143.420 Y95.251 E0.01376 ; perimeter

G1 X143.384 Y95.094 E0.01377 ; perimeter

G1 X143.297 Y94.967 E0.01379 ; perimeter

G1 X143.192 Y94.899 E0.01380 ; perimeter

G1 X143.071 Y94.868 E0.01382 ; perimeter

G1 X142.947 Y94.878 E0.01383 ; perimeter

G1 X142.787 Y94.963 E0.01385 ; perimeter

G1 X142.696 Y95.094 E0.01387 ; perimeter

G1 X142.660 Y95.251 E0.01388 ; perimeter

G1 X142.652 Y115.302 E0.01599 ; perimeter

G1 X142.613 Y115.426 E0.01600 ; perimeter

G1 X142.519 Y115.537 E0.01602 ; perimeter

G1 X142.432 Y115.593 E0.01603 ; perimeter

G1 X142.332 Y115.619 E0.01604 ; perimeter

G1 X142.208 Y115.616 E0.01605 ; perimeter

G1 X142.073 Y115.563 E0.01607 ; perimeter

G1 X141.981 Y115.479 E0.01608 ; perimeter

G1 X141.921 Y115.369 E0.01609 ; perimeter

G1 X141.900 Y115.235 E0.01611 ; perimeter

G1 X141.900 Y95.257 E0.01821 ; perimeter

G1 X141.879 Y95.123 E0.01822 ; perimeter

G1 X141.819 Y95.013 E0.01824 ; perimeter

G1 X141.723 Y94.925 E0.01825 ; perimeter

G1 X141.551 Y94.868 E0.01827 ; perimeter

G1 X141.422 Y94.879 E0.01828 ; perimeter

G1 X141.263 Y94.967 E0.01830 ; perimeter

G1 X141.187 Y95.065 E0.01831 ; perimeter

G1 X141.140 Y95.251 E0.01833 ; perimeter

G1 X141.140 Y115.235 E0.02043 ; perimeter

G1 X141.119 Y115.369 E0.02045 ; perimeter

G1 X141.044 Y115.494 E0.02046 ; perimeter

G1 X140.967 Y115.563 E0.02048 ; perimeter

G1 X140.873 Y115.606 E0.02049 ; perimeter

G1 X140.750 Y115.623 E0.02050 ; perimeter

G1 X140.590 Y115.581 E0.02052 ; perimeter

G1 X140.483 Y115.500 E0.02053 ; perimeter

G1 X140.401 Y115.369 E0.02055 ; perimeter

G1 X140.384 Y115.267 E0.02056 ; perimeter

G1 X140.380 Y95.251 E0.02266 ; perimeter

G1 X140.348 Y95.104 E0.02268 ; perimeter

G1 X140.284 Y94.998 E0.02269 ; perimeter

G1 X140.178 Y94.915 E0.02270 ; perimeter

G1 X140.031 Y94.868 E0.02272 ; perimeter

G1 X139.907 Y94.878 E0.02273 ; perimeter

G1 X139.743 Y94.966 E0.02275 ; perimeter

G1 X139.641 Y95.123 E0.02277 ; perimeter

G1 X139.620 Y95.257 E0.02279 ; perimeter

G1 X139.620 Y115.235 E0.02489 ; perimeter

G1 X139.599 Y115.369 E0.02490 ; perimeter

G1 X139.539 Y115.479 E0.02491 ; perimeter

G1 X139.447 Y115.563 E0.02493 ; perimeter

G1 X139.333 Y115.613 E0.02494 ; perimeter

G1 X139.209 Y115.624 E0.02495 ; perimeter

G1 X139.062 Y115.575 E0.02497 ; perimeter

G1 X138.963 Y115.501 E0.02498 ; perimeter

G1 X138.881 Y115.366 E0.02500 ; perimeter

G1 X138.860 Y115.235 E0.02501 ; perimeter

G1 X138.860 Y95.257 E0.02711 ; perimeter

G1 X138.839 Y95.123 E0.02713 ; perimeter

G1 X138.779 Y95.013 E0.02714 ; perimeter

G1 X138.683 Y94.925 E0.02715 ; perimeter

G1 X138.511 Y94.868 E0.02717 ; perimeter

G1 X138.387 Y94.878 E0.02719 ; perimeter

G1 X138.223 Y94.966 E0.02721 ; perimeter

G1 X138.121 Y95.123 E0.02723 ; perimeter

G1 X138.100 Y95.256 E0.02724 ; perimeter

G1 X138.100 Y115.235 E0.02934 ; perimeter

G1 X138.079 Y115.369 E0.02935 ; perimeter

G1 X138.016 Y115.483 E0.02937 ; perimeter

G1 X137.872 Y115.593 E0.02939 ; perimeter

G1 X137.751 Y115.624 E0.02940 ; perimeter

G1 X137.622 Y115.612 E0.02941 ; perimeter

G1 X137.532 Y115.572 E0.02942 ; perimeter

G1 X137.436 Y115.493 E0.02944 ; perimeter

G1 X137.372 Y115.388 E0.02945 ; perimeter

G1 X137.344 Y115.267 E0.02946 ; perimeter

G1 X137.340 Y95.257 E0.03157 ; perimeter

G1 X137.319 Y95.123 E0.03158 ; perimeter

G1 X137.221 Y94.970 E0.03160 ; perimeter

G1 X137.111 Y94.901 E0.03161 ; perimeter

G1 X136.991 Y94.870 E0.03163 ; perimeter

G1 X136.868 Y94.881 E0.03164 ; perimeter

G1 X136.708 Y94.964 E0.03166 ; perimeter

G1 X136.628 Y95.066 E0.03167 ; perimeter

G1 X136.580 Y95.251 E0.03169 ; perimeter

G1 X136.574 Y115.308 E0.03380 ; perimeter

G1 X136.533 Y115.426 E0.03381 ; perimeter

G1 X136.412 Y115.561 E0.03383 ; perimeter

G1 X136.293 Y115.613 E0.03384 ; perimeter

G1 X136.169 Y115.624 E0.03386 ; perimeter

G1 X136.048 Y115.593 E0.03387 ; perimeter

G1 X135.939 Y115.521 E0.03388 ; perimeter

G1 X135.841 Y115.369 E0.03390 ; perimeter

G1 X135.820 Y115.235 E0.03392 ; perimeter

G1 X135.820 Y95.257 E0.03602 ; perimeter

G1 X135.799 Y95.123 E0.03603 ; perimeter

G1 X135.717 Y94.992 E0.03605 ; perimeter

G1 X135.562 Y94.890 E0.03607 ; perimeter

G1 X135.430 Y94.870 E0.03608 ; perimeter

G1 X135.292 Y94.896 E0.03610 ; perimeter

G1 X135.180 Y94.972 E0.03611 ; perimeter

G1 X135.094 Y95.098 E0.03613 ; perimeter

G1 X135.060 Y95.251 E0.03614 ; perimeter

G1 X135.058 Y115.235 E0.03824 ; perimeter

G1 X135.037 Y115.368 E0.03826 ; perimeter

G1 X134.978 Y115.478 E0.03827 ; perimeter

G1 X134.881 Y115.564 E0.03828 ; perimeter

G1 X134.711 Y115.622 E0.03830 ; perimeter

G1 X134.588 Y115.610 E0.03832 ; perimeter

G1 X134.473 Y115.563 E0.03833 ; perimeter

G1 X134.381 Y115.479 E0.03834 ; perimeter

G1 X134.317 Y115.348 E0.03836 ; perimeter

G1 X134.300 Y115.235 E0.03837 ; perimeter

G1 X134.300 Y95.251 E0.04047 ; perimeter

G1 X134.253 Y95.065 E0.04049 ; perimeter

G1 X134.177 Y94.967 E0.04050 ; perimeter

G1 X134.043 Y94.890 E0.04052 ; perimeter

G1 X133.910 Y94.870 E0.04053 ; perimeter

G1 X133.788 Y94.893 E0.04055 ; perimeter

G1 X133.660 Y94.971 E0.04056 ; perimeter

G1 X133.561 Y95.123 E0.04058 ; perimeter

G1 X133.540 Y95.257 E0.04059 ; perimeter

G1 X133.540 Y115.235 E0.04269 ; perimeter

G1 X133.519 Y115.369 E0.04271 ; perimeter

G1 X133.459 Y115.479 E0.04272 ; perimeter

G1 X133.367 Y115.563 E0.04273 ; perimeter

G1 X133.252 Y115.610 E0.04275 ; perimeter

```
G1 X133.129 Y115.622 E0.04276 ; perimeter

G1 X133.009 Y115.590 E0.04277 ; perimeter

G1 X132.903 Y115.525 E0.04279 ; perimeter

G1 X132.826 Y115.425 E0.04280 ; perimeter

G1 X132.780 Y115.237 E0.04282 ; perimeter

G1 X132.780 Y90.246 E0.04545 ; perimeter

G92 E0 ; reset extrusion distance

M107 T10  ; turn off fans and lasers

M104 S0    ; turn off temperature

M140 S0   ;turn off the hot bed.

G91          ;

G1 Z5.0     ; Drop bed 5mm for extra clearance

G90          ; absolute

G28 X0 Y0  ; home X axis

G92 X0 Y0 ; confirm we are at zero

M84          ; disable motors

M30          ; End ofprogram

; filament used = 0.0mm (0.0cm3)


; avoid_crossing_perimeters = 1

; bed_shape = 0x0,275x0,275x225,0x225

; bed_temperature = 0

; before_layer_gcode = ;announce new layer <[layer_num]>\n;---\nM756
S[layer_height]\nM790 ;execute any new layer actions\n;---

; bridge_acceleration = 0

; bridge_fan_speed = 100

; brim_width = 0

; complete_objects = 0

; cooling = 1
```

; default_acceleration = 0

; disable_fan_first_layers = 3

; duplicate_distance = 6

; end_gcode = M107 T10 ; turn off fans and lasers\nM104 S0 ; turn off temperature\nM140 S0 ;turn off the hot bed.\nG91 ;\nG1 Z5.0 ; Drop bed 5mm for extra clearance \nG90 ; absolute\nG28 X0 Y0 ; home X axis\nG92 X0 Y0 ; confirm we are at zero\nM84 ; disable motors\nM30 ; End ofprogram

; extruder_clearance_height = 20

; extruder_clearance_radius = 20

; extruder_offset = 0x0,0x0,0x0,0x0

; extrusion_axis = E

; extrusion_multiplier = 1

; fan_always_on = 0

; fan_below_layer_time = 60

; filament_colour = #FFFFFF

; filament_diameter = 17

; first_layer_acceleration = 0

; first_layer_bed_temperature = 0

; first_layer_extrusion_width = 0.26

; first_layer_speed = 1.5

; first_layer_temperature = 0

; gcode_arcs = 0

; gcode_comments = 1

; gcode_flavor = reprap

; infill_acceleration = 0

; infill_first = 0

; layer_gcode =

; max_fan_speed = 100

; max_print_speed = 30

; max_volumetric_speed = 0

; min_fan_speed = 35

; min_print_speed = 10

; min_skirt_length = 0

; notes =

; nozzle_diameter = 0.26,0.26,0.31,0.06

; only_retract_when_crossing_perimeters = 1

; ooze_prevention = 0

; output_filename_format = [input_filename_base].gcode

; perimeter_acceleration = 0

; post_process =

; pressure_advance = 0

; resolution = 0

; retract_before_travel = 2,1,2,2

; retract_layer_change = 1,0,0,0

; retract_length = 0,0,0,0

; retract_length_toolchange = 0,0,0,0

; retract_lift = 0,0,0,0

; retract_restart_extra = 0,0,0,0

; retract_restart_extra_toolchange = 0,0,0,0

; retract_speed = 40,40,40,40

; skirt_distance = 5

; skirt_height = 0

; skirts = 0

; slowdown_below_layer_time = 5

; spiral_vase = 0

; standby_temperature_delta = -5

; start_gcode = M104 T10 S[temperature]\nG21 ; use millimeters\nG90 ; absolute coordinates\nG0 Z5 ; lift head to avoid collisions\nG28 X0 Y0 ; home X and Y\nG92 X0 Y0 ; reset origin: X and Y\nG0 X0 Y0 ; move to desired origin\nG92 X0 Y0 ; reset origin: X and Y\nM83

; relative extruder coordinates\n;M109 S[temperature] ;wait for temperture to come up.\nM756 S[first_layer_height] ;set flowfor the first layer please\n\n

; temperature = 0

; threads = 8

; toolchange_gcode =

; travel_speed = 20

; use_firmware_retraction = 0

; use_relative_e_distances = 0

; use_volumetric_e = 0

; vibration_limit = 0

; wipe = 0,0,0,0

; z_offset = 0

; dont_support_bridges = 0

; extrusion_width = 0.26

; first_layer_height = 0.1

; infill_only_where_needed = 0

; interface_shells = 0

; layer_height = 0.1

; raft_layers = 0

; seam_position = aligned

; support_material = 0

; support_material_angle = 0

; support_material_contact_distance = 0.2

; support_material_enforce_layers = 0

; support_material_extruder = 1

; support_material_extrusion_width = 0

; support_material_interface_extruder = 1

; support_material_interface_layers = 3

; support_material_interface_spacing = 0

; support_material_interface_speed = 100%

; support_material_pattern = pillars

; support_material_spacing = 2.5

; support_material_speed = 20

; support_material_threshold = 35

; xy_size_compensation = 0

; bottom_solid_layers = 1

; bridge_flow_ratio = 1

; bridge_speed = 1.5

; external_fill_pattern = rectilinear

; external_perimeter_extrusion_width = 0.26

; external_perimeter_speed = 1.5

; external_perimeters_first = 0

; extra_perimeters = 0

; fill_angle = 45

; fill_density = 100%

; fill_pattern = rectilinear

; gap_fill_speed = 1.5

; infill_every_layers = 1

; infill_extruder = 1

; infill_extrusion_width = 0.26

; infill_overlap = 15%

; infill_speed = 1.5

; overhangs = 1

; perimeter_extruder = 1

; perimeter_extrusion_width = 0.26

; perimeter_speed = 1.5

; perimeters = 1

; small_perimeter_speed = 1.5

; solid_infill_below_area = 9

; solid_infill_every_layers = 1

; solid_infill_extruder = 1

; solid_infill_extrusion_width = 0.26

; solid_infill_speed = 1.5

; thin_walls = 1

; top_infill_extrusion_width = 0.26

; top_solid_infill_speed = 1.5

; top_solid_layers = 1

G code for second strain gauge printed using Bare Conductive ink

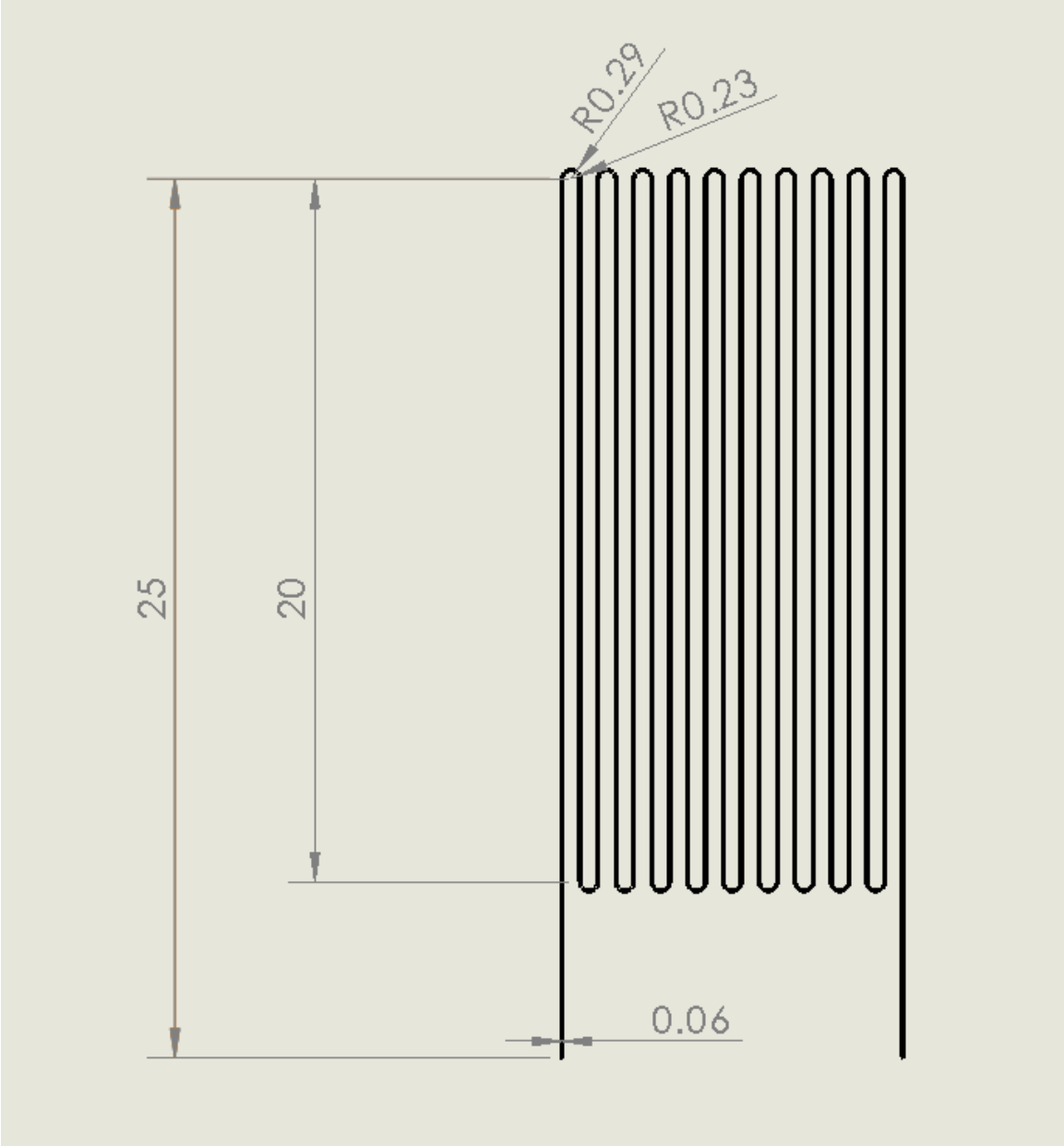

Measurements in mm

; generated by Slic3r 1.2.9 on 2018-03-22 at 19:11:29

; external perimeters extrusion width = 0.06mm

; perimeters extrusion width = 0.06mm

; infill extrusion width = 0.06mm

; solid infill extrusion width = 0.06mm

; top infill extrusion width = 0.06mm

```
M107 ; disable fan
M104 T10  S0
G21     ; use millimeters
G90     ; absolute coordinates
G0 Z5 ; lift head to avoid collisions
G28 X0 Y0 ; home X and Y
G92 X0 Y0 ; reset origin: X and Y
G0 X0 Y0   ; move to desired origin
G92 X0 Y0 ; reset origin: X and Y
M83         ; relative extruder coordinates
;M109 S0  ;wait for temperture to come up.
M756 S0.06  ;set flowfor the first layer please



G21 ; set units to millimeters
G90 ; use absolute coordinates
M82 ; use absolute distances for extrusion
G92 E0 ; reset extrusion distance
;announce new layer <0>
;---
M756 S0.06
M790 ;execute any new layer actions
;---
G1 Z0.060 F1200.000 ; move to next layer (0)
G1 X120 Y80
G1 X120 Y130 E1
G1 X160 Y130 E1
```

G1 X160 Y80 E1

G1 X144.845 Y90.358 E1 F1200.000 ; move to first perimeter point

G1 X144.839 Y115.355 E0.00031 F210.000 ; perimeter

G1 X144.831 Y115.441 E0.00031 ; perimeter

G1 X144.791 Y115.514 E0.00031 ; perimeter

G1 X144.697 Y115.585 E0.00031 ; perimeter

G1 X144.609 Y115.606 E0.00032 ; perimeter

G1 X144.529 Y115.605 E0.00032 ; perimeter

G1 X144.421 Y115.542 E0.00032 ; perimeter

G1 X144.354 Y115.437 E0.00032 ; perimeter

G1 X144.335 Y115.355 E0.00032 ; perimeter

G1 X144.335 Y95.360 E0.00057 ; perimeter

G1 X144.321 Y95.276 E0.00057 ; perimeter

G1 X144.252 Y95.170 E0.00057 ; perimeter

G1 X144.102 Y95.104 E0.00057 ; perimeter

G1 X143.977 Y95.125 E0.00058 ; perimeter

G1 X143.907 Y95.170 E0.00058 ; perimeter

G1 X143.857 Y95.236 E0.00058 ; perimeter

G1 X143.825 Y95.362 E0.00058 ; perimeter

G1 X143.825 Y115.354 E0.00083 ; perimeter

G1 X143.793 Y115.480 E0.00083 ; perimeter

G1 X143.738 Y115.541 E0.00083 ; perimeter

G1 X143.672 Y115.591 E0.00083 ; perimeter

G1 X143.556 Y115.610 E0.00083 ; perimeter

G1 X143.460 Y115.585 E0.00084 ; perimeter

G1 X143.372 Y115.512 E0.00084 ; perimeter

G1 X143.333 Y115.439 E0.00084 ; perimeter

G1 X143.313 Y115.315 E0.00084 ; perimeter

G1 X143.315 Y95.360 E0.00109 ; perimeter

G1 X143.301 Y95.275 E0.00109 ; perimeter

G1 X143.259 Y95.204 E0.00109 ; perimeter

G1 X143.158 Y95.130 E0.00109 ; perimeter

G1 X143.082 Y95.104 E0.00109 ; perimeter

G1 X142.981 Y95.119 E0.00109 ; perimeter

G1 X142.888 Y95.170 E0.00110 ; perimeter

G1 X142.822 Y95.277 E0.00110 ; perimeter

G1 X142.805 Y95.360 E0.00110 ; perimeter

G1 X142.791 Y115.441 E0.00135 ; perimeter

G1 X142.689 Y115.571 E0.00135 ; perimeter

G1 X142.613 Y115.605 E0.00135 ; perimeter

G1 X142.495 Y115.603 E0.00135 ; perimeter

G1 X142.349 Y115.514 E0.00135 ; perimeter

G1 X142.309 Y115.441 E0.00136 ; perimeter

G1 X142.293 Y115.319 E0.00136 ; perimeter

G1 X142.295 Y95.360 E0.00161 ; perimeter

G1 X142.234 Y95.199 E0.00161 ; perimeter

G1 X142.142 Y95.125 E0.00161 ; perimeter

G1 X142.061 Y95.104 E0.00161 ; perimeter

G1 X141.945 Y95.125 E0.00161 ; perimeter

G1 X141.867 Y95.171 E0.00161 ; perimeter

G1 X141.812 Y95.248 E0.00161 ; perimeter

G1 X141.785 Y95.361 E0.00162 ; perimeter

G1 X141.771 Y115.441 E0.00187 ; perimeter

G1 X141.669 Y115.571 E0.00187 ; perimeter

G1 X141.593 Y115.605 E0.00187 ; perimeter

G1 X141.475 Y115.605 E0.00187 ; perimeter

G1 X141.337 Y115.520 E0.00187 ; perimeter

G1 X141.275 Y115.354 E0.00187 ; perimeter

G1 X141.275 Y95.361 E0.00212 ; perimeter

G1 X141.254 Y95.265 E0.00213 ; perimeter

G1 X141.192 Y95.170 E0.00213 ; perimeter

G1 X141.042 Y95.104 E0.00213 ; perimeter

G1 X140.917 Y95.125 E0.00213 ; perimeter

G1 X140.847 Y95.170 E0.00213 ; perimeter

G1 X140.797 Y95.236 E0.00213 ; perimeter

G1 X140.765 Y95.362 E0.00213 ; perimeter

G1 X140.751 Y115.441 E0.00238 ; perimeter

G1 X140.711 Y115.514 E0.00239 ; perimeter

G1 X140.618 Y115.587 E0.00239 ; perimeter

G1 X140.457 Y115.605 E0.00239 ; perimeter

G1 X140.308 Y115.510 E0.00239 ; perimeter

G1 X140.271 Y115.435 E0.00239 ; perimeter

G1 X140.253 Y115.319 E0.00239 ; perimeter

G1 X140.260 Y95.372 E0.00264 ; perimeter

G1 X140.196 Y95.199 E0.00264 ; perimeter

G1 X140.116 Y95.131 E0.00265 ; perimeter

G1 X140.022 Y95.104 E0.00265 ; perimeter

G1 X139.921 Y95.119 E0.00265 ; perimeter

G1 X139.827 Y95.170 E0.00265 ; perimeter

G1 X139.765 Y95.270 E0.00265 ; perimeter

G1 X139.745 Y95.362 E0.00265 ; perimeter

G1 X139.741 Y115.400 E0.00290 ; perimeter

G1 X139.714 Y115.479 E0.00290 ; perimeter

G1 X139.662 Y115.543 E0.00290 ; perimeter

G1 X139.551 Y115.605 E0.00291 ; perimeter

G1 X139.471 Y115.609 E0.00291 ; perimeter

G1 X139.353 Y115.565 E0.00291 ; perimeter

G1 X139.289 Y115.514 E0.00291 ; perimeter

G1 X139.249 Y115.441 E0.00291 ; perimeter

G1 X139.233 Y115.319 E0.00291 ; perimeter

G1 X139.235 Y95.360 E0.00316 ; perimeter

G1 X139.181 Y95.203 E0.00316 ; perimeter

G1 X139.081 Y95.124 E0.00316 ; perimeter

G1 X139.002 Y95.107 E0.00316 ; perimeter

G1 X138.879 Y95.131 E0.00317 ; perimeter

G1 X138.808 Y95.170 E0.00317 ; perimeter

G1 X138.742 Y95.277 E0.00317 ; perimeter

G1 X138.725 Y95.360 E0.00317 ; perimeter

G1 X138.723 Y115.354 E0.00342 ; perimeter

G1 X138.667 Y115.517 E0.00342 ; perimeter

G1 X138.572 Y115.590 E0.00342 ; perimeter

G1 X138.492 Y115.609 E0.00342 ; perimeter

G1 X138.400 Y115.599 E0.00342 ; perimeter

G1 X138.300 Y115.542 E0.00343 ; perimeter

G1 X138.247 Y115.479 E0.00343 ; perimeter

G1 X138.221 Y115.400 E0.00343 ; perimeter

G1 X138.215 Y95.360 E0.00368 ; perimeter

G1 X138.198 Y95.277 E0.00368 ; perimeter

G1 X138.132 Y95.170 E0.00368 ; perimeter

G1 X138.062 Y95.125 E0.00368 ; perimeter

G1 X137.946 Y95.106 E0.00368 ; perimeter

G1 X137.863 Y95.125 E0.00368 ; perimeter

G1 X137.765 Y95.198 E0.00369 ; perimeter

G1 X137.705 Y95.361 E0.00369 ; perimeter

G1 X137.701 Y115.400 E0.00394 ; perimeter

G1 X137.665 Y115.494 E0.00394 ; perimeter

G1 X137.592 Y115.567 E0.00394 ; perimeter

G1 X137.516 Y115.600 E0.00394 ; perimeter

G1 X137.395 Y115.605 E0.00394 ; perimeter

G1 X137.250 Y115.509 E0.00394 ; perimeter

G1 X137.209 Y115.439 E0.00395 ; perimeter

G1 X137.193 Y115.319 E0.00395 ; perimeter

G1 X137.195 Y95.360 E0.00420 ; perimeter

G1 X137.178 Y95.277 E0.00420 ; perimeter

G1 X137.112 Y95.170 E0.00420 ; perimeter

G1 X137.042 Y95.125 E0.00420 ; perimeter

G1 X136.962 Y95.107 E0.00420 ; perimeter

G1 X136.837 Y95.125 E0.00420 ; perimeter

G1 X136.769 Y95.173 E0.00420 ; perimeter

G1 X136.720 Y95.237 E0.00420 ; perimeter

G1 X136.685 Y95.362 E0.00421 ; perimeter

G1 X136.683 Y115.354 E0.00445 ; perimeter

G1 X136.627 Y115.517 E0.00446 ; perimeter

G1 X136.532 Y115.590 E0.00446 ; perimeter

G1 X136.451 Y115.609 E0.00446 ; perimeter

G1 X136.369 Y115.605 E0.00446 ; perimeter

G1 X136.259 Y115.541 E0.00446 ; perimeter

G1 X136.207 Y115.479 E0.00446 ; perimeter

G1 X136.181 Y115.400 E0.00446 ; perimeter

G1 X136.175 Y95.362 E0.00471 ; perimeter

G1 X136.155 Y95.270 E0.00471 ; perimeter

G1 X136.093 Y95.170 E0.00472 ; perimeter

G1 X136.022 Y95.125 E0.00472 ; perimeter

```
G1 X135.906 Y95.107 E0.00472 ; perimeter
G1 X135.748 Y95.170 E0.00472 ; perimeter
G1 X135.679 Y95.276 E0.00472 ; perimeter
G1 X135.665 Y95.360 E0.00472 ; perimeter
G1 X135.663 Y115.355 E0.00497 ; perimeter
G1 X135.616 Y115.503 E0.00497 ; perimeter
G1 X135.552 Y115.567 E0.00498 ; perimeter
G1 X135.465 Y115.605 E0.00498 ; perimeter
G1 X135.347 Y115.605 E0.00498 ; perimeter
G1 X135.271 Y115.571 E0.00498 ; perimeter
G1 X135.211 Y115.513 E0.00498 ; perimeter
G1 X135.173 Y115.439 E0.00498 ; perimeter
G1 X135.155 Y115.315 E0.00498 ; perimeter
G1 X135.155 Y90.358 E0.00529 ; perimeter

G92 E0 ; reset extrusion distance
M107 T10  ; turn off fans and lasers
M104 S0    ; turn off temperature
M140 S0   ;turn off the hot bed.
G91          ;
G1 Z5.0     ; Drop bed 5mm for extra clearance
G90          ; absolute
G28 X0 Y0  ; home X axis
G92 X0 Y0 ; confirm we are at zero
M84          ; disable motors
M30          ; End ofprogram
; filament used = 0.0mm (0.0cm3)

; avoid_crossing_perimeters = 1
```

; bed_shape = 0x0,275x0,275x225,0x225

; bed_temperature = 0

; before_layer_gcode = ;announce new layer <[layer_num]>\n;---\nM756 S[layer_height]\nM790 ;execute any new layer actions\n;---

; bridge_acceleration = 0

; bridge_fan_speed = 100

; brim_width = 0

; complete_objects = 0

; cooling = 1

; default_acceleration = 0

; disable_fan_first_layers = 3

; duplicate_distance = 6

; end_gcode = M107 T10 ; turn off fans and lasers\nM104 S0 ; turn off temperature\nM140 S0 ;turn off the hot bed.\nG91 ;\nG1 Z5.0 ; Drop bed 5mm for extra clearance \nG90 ; absolute\nG28 X0 Y0 ; home X axis\nG92 X0 Y0 ; confirm we are at zero\nM84 ; disable motors\nM30 ; End ofprogram

; extruder_clearance_height = 20

; extruder_clearance_radius = 20

; extruder_offset = 0x0,0x0,0x0,0x0

; extrusion_axis = E

; extrusion_multiplier = 1

; fan_always_on = 0

; fan_below_layer_time = 60

; filament_colour = #FFFFFF

; filament_diameter = 17

; first_layer_acceleration = 0

; first_layer_bed_temperature = 0

; first_layer_extrusion_width = 0.06

; first_layer_speed = 3.5

; first_layer_temperature = 0

; gcode_arcs = 0

; gcode_comments = 1

; gcode_flavor = reprap

; infill_acceleration = 0

; infill_first = 0

; layer_gcode =

; max_fan_speed = 100

; max_print_speed = 30

; max_volumetric_speed = 0

; min_fan_speed = 35

; min_print_speed = 10

; min_skirt_length = 0

; notes =

; nozzle_diameter = 0.06,0.06,0.31,0.06

; only_retract_when_crossing_perimeters = 1

; ooze_prevention = 0

; output_filename_format = [input_filename_base].gcode

; perimeter_acceleration = 0

; post_process =

; pressure_advance = 0

; resolution = 0

; retract_before_travel = 2,1,2,2

; retract_layer_change = 1,0,0,0

; retract_length = 0,0,0,0

; retract_length_toolchange = 0,0,0,0

; retract_lift = 0,0,0,0

; retract_restart_extra = 0,0,0,0

; retract_restart_extra_toolchange = 0,0,0,0

; retract_speed = 40,40,40,40

; skirt_distance = 5

; skirt_height = 0

; skirts = 0

; slowdown_below_layer_time = 5

; spiral_vase = 0

; standby_temperature_delta = -5

; start_gcode = M104 T10 S[temperature]\nG21   ; use millimeters\nG90   ; absolute coordinates\nG0 Z5 ; lift head to avoid collisions\nG28 X0 Y0 ; home X and Y\nG92 X0 Y0 ; reset origin: X and Y\nG0 X0 Y0   ; move to desired origin\nG92 X0 Y0 ; reset origin: X and Y\nM83 ; relative extruder coordinates\n;M109 S[temperature] ;wait for temperture to come up.\nM756 S[first_layer_height] ;set flowfor the first layer please\n\n

; temperature = 0

; threads = 8

; toolchange_gcode =

; travel_speed = 20

; use_firmware_retraction = 0

; use_relative_e_distances = 0

; use_volumetric_e = 0

; vibration_limit = 0

; wipe = 0,0,0,0

; z_offset = 0

; dont_support_bridges = 0

; extrusion_width = 0.06

; first_layer_height = 0.06

; infill_only_where_needed = 0

; interface_shells = 0

; layer_height = 0.06

; raft_layers = 0

; seam_position = aligned

; support_material = 0

; support_material_angle = 0

; support_material_contact_distance = 0.2

; support_material_enforce_layers = 0

; support_material_extruder = 1

; support_material_extrusion_width = 0

; support_material_interface_extruder = 1

; support_material_interface_layers = 3

; support_material_interface_spacing = 0

; support_material_interface_speed = 100%

; support_material_pattern = pillars

; support_material_spacing = 2.5

; support_material_speed = 20

; support_material_threshold = 35

; xy_size_compensation = 0

; bottom_solid_layers = 1

; bridge_flow_ratio = 1

; bridge_speed = 3.5

; external_fill_pattern = rectilinear

; external_perimeter_extrusion_width = 0.06

; external_perimeter_speed = 3.5

; external_perimeters_first = 0

; extra_perimeters = 0

; fill_angle = 45

; fill_density = 100%

; fill_pattern = rectilinear

; gap_fill_speed = 3.5

; infill_every_layers = 1

; infill_extruder = 1

; infill_extrusion_width = 0.06

; infill_overlap = 15%

; infill_speed = 3.5

; overhangs = 1

; perimeter_extruder = 1

; perimeter_extrusion_width = 0.06

; perimeter_speed = 3.5

; perimeters = 1

; small_perimeter_speed = 3.5

; solid_infill_below_area = 9

; solid_infill_every_layers = 1

; solid_infill_extruder = 1

; solid_infill_extrusion_width = 0.06

; solid_infill_speed = 3.5

; thin_walls = 1

; top_infill_extrusion_width = 0.06

; top_solid_infill_speed = 3.5

; top_solid_layers = 1